illumination, [1–3] corneal epithelial damage by ultraviolet (UV) irradiation, [4] retinal cell damage by light from an operating microscope or endoillumination during vitreous surgery, [5–8] and macular damage by a laser pointer [9]. Most of these injuries were caused by unnatural conditions, namely high intensities or long durations of the irradiation.

Commercially available photographic flash units for cameras were developed over a century ago so that photography could be performed under reduced light levels. They are generally considered to be safe because of their extremely short flash duration. However, the well-known after-images suggest that they do have a long-lasting effect on the retina, and the instruction manuals for the flash units warn users of the possibility of injury by firing the flash close to the eye. However, very few studies have been done to examine the phototoxicity of such flash units for cameras.

The aim of this study was to determine whether flashes from a commercially available photographic flash lamp can damage ocular tissues. The eyes of rats were exposed to different number of flashes from a commercially available photographic flash unit, and both morphological and physiological techniques were used to assess the cornea and retina.

Materials and methods

Animals and light exposure

All animals were cared for in accordance with the Statement by the Association of Research in Vision and Ophthalmology for the Use of Animals in Ophthalmic and Vision Research, and all research procedures were performed in compliance with the regulations on animal usage by Keio University, Tokyo, Japan.

Male Sprague–Dawley rats, weighing 150–200 g and 6- to 8-week-old, were anesthetized with an intramuscular injection of 100 mg/kg of ketamine and 10 mg/kg of xylazine. The right eyes were exposed to the photographic flash bulb (19196 OPTICAM 16M, Fujikoeki, Japan), but the left eyes were blocked from the light by an aluminum sheet and used for control. The flash bulb was placed 0.1, 1, or 3 m from the eye, and the number of flashes delivered was 10, 100, or 1,000 with an interflash interval of 5 s that was controlled by a personal computer (FMV, Fujitsu, Japan). During the exposures, rats were placed on a heating pad, and the body temperature was maintained at 36°C throughout the experiment. The corneas of both eyes were kept moist by frequent application of balanced salt solution and hydroxymethyl cellulose during and after the light exposure. A speculum was not used, but the eyes were kept widely opened to expose the light to the whole eye during the light exposure. Each rat was anesthetized for the same duration of 1.5 h, and supplemented by one-half of the original dose of ketamine and xylazine when the rat began to move. This duration of 1.5 h was equal to the maximal exposure of 1,000 times of flashes with an interval of 5 s. After the exposure to the flashes from the OPTICAM, the ocular surface was protected by application of an antibiotic ointment.

All animals were kept in the animal rooms for several days after they were received from the animal dealer. The luminance in the animal room at the cage level was 800 lux, and the lighting was set on a 12:12 h light:dark schedule. After animals were exposed to the flashes, they were returned to a darkened room because all experiments were done at night.

The photographic flash bulb (19196 OPTICAM 16M, Fujikoeki, Japan, color temperature 5,700 K; flash duration 0.5 ms) is a xenon bulb and emits light throughout the visible spectrum. A UV filter is incorporated in the unit to attenuate wavelengths below 380 nm. The spectral energy in a single flash of the xenon bulb ($n = 2$) was recorded with a spectroradiometer (USR-40V, Ushio Electronics, Japan) that was responsive to wavelengths 300–1,100 nm placed 5 cm from the flash unit.

Fluorescein staining score for corneal epithelial damage

Corneal epithelial damage was assessed by scoring the degree of fluorescein staining before, 24 h, and 7 days after the light exposure

Table 1 The experimental design and the numbers of the rats for the flash light exposure

Situation	Distance	Count	Fluorescein	ERG
Unusual	0.1 m	1,000	5	5
Usual	1 m	1,000	3	4
Usual	1 m	100	3	3
Usual	1 m	10	3	3
Usual	3 m	1,000	3	4
Usual	3 m	100	3	3
Usual	3 m	10	3	3
Control	No flash	0	3	3

Situation, the maximal exposure represents unusual accidental exposure. distance; the distance form the flash bulb to the rat eye, count; the numbers of flash light exposure, fluorescein; the numbers of the eyes examed in fluorescein score, ERG; the numbers of the eyes examed in electroretinograms. The three rats in condition of 1,000 flash at 0.1 m were sacrificed on the next day, but the rest of three rats were killed after 1 week

(Table 1). To do this, 10 μl of a 10% fluorescein solution was dropped on the cornea, and the excess dye was quickly washed out by balanced salt solution. The degree of fluorescein staining observed with a slit-lamp biomicroscope was scored from 0 to 3 with; 0 = no stain, 1 = slight stain with one spot of fluorescein, 2 = moderate stain with two or three spots of fluorescein, and 3 = severe stain with more than four spots of fluorescein (Fig. 1). The superior, central, and inferior regions of the cornea were scored separately, and the final score was the sum of these three regions with a range from 0 to 9. In addition, the degree of cataract was also evaluated by slit-lamp biomicroscopy.

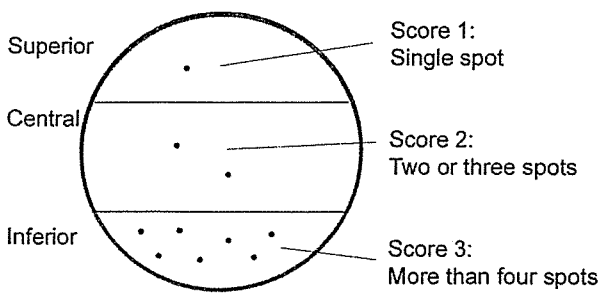

Fig. 1 Scoring of fluorescein score. The superior, central, and inferior regions of the cornea were scored separately, and the final score was the sum of these three regions with a range from 0 to 9

Electroretinography

Electroretinograms (ERGs) were recorded from both eyes simultaneously after more than 6 h of dark-adaptation before and 24 h after the light exposure (Table 1). ERGs were also recorded 7 days after the exposure to the maximum energy (1,000 flashes at 0.1 m). After anesthesia with an intramuscular injection of a mixture of ketamine (100 mg/kg) and xylazine (10 mg/kg), the pupils in both eyes were dilated with 10μl of 0.5% tropicamide and 0.5% of phenylephrine. The rats were placed on a heating pad, and the body temperature was maintained at 36°C throughout the experiment.

The cornea was anesthetized with topical benoxylchloride, and a contact lens electrode carrying white light-emitting diodes (LEDs; Kyoto Contact, Kyoto, Japan) was used to elicit and record the ERGs by a single flash of 10,000 cd-s/m^2 luminance in the dark with a stimulus duration of 5 ms. The reference electrode was a needle placed subcutaneously between the eyes, and another needle electrode was placed subcutaneously in the neck region as the ground electrode. Responses were differentially amplified and filtered with digital bandpass filters set at 0.5–200 Hz to record the a- and b-waves (Neuropack μ system, Nihon Koden, Tokyo, Japan). The amplitude of the a-wave or b-wave of the ERG of the affected right eye was compared to the amplitude of the same eye before light exposure and the amplitude ratios of after/before exposure of the ERG components were calculated.

Morphological evaluations

The animals were killed 24 h or a week after the light exposure by an intraperitoneal injection of sodium pentobarbital. The eyes were enucleated and the anterior segment was cut-off. The cornea was fixed in phosphate-buffered 2.5% glutaraldehyde and processed for scanning electron microscopy (SEM; S-4000, HITACHI, Japan). The eyecup was fixed in 4% paraformaldehyde overnight, embedded in paraffin, sectioned at 5μm, and stained with hematoxlyin and eosin for light microscopy. The superior

central and temporal retina has been described to be more susceptible than other areas [10, 11]. The thickness of outer nuclear layer (ONL) and sensory retina was measured from the histological section at approximately 1 mm temporal or superior to the optic disc with a width of 500μm in the experimental and control eyes ($n = 3$). The column cell count of the ONL nuclei (cell count) was also measured in the same histological sections.

To detect apoptotic cells, the terminal deoxynucleotidyl transferase (TdT)-mediated, dUTP-biotin catalyzed DNA nick-end labeling (TUNEL) method was used (In situ apoptosis detection kit, Takara, Japan). The TUNEL enzyme (1 h at 37°C) and peroxidase converter (30 min at 37°C) were applied to the sections after the sections were incubated in a permeabilizing solution of 0.1%Triton-X in 0.1% sodium citrate for 2 min on ice. DAB was used as the chromogen. TUNEL-positive cells were counted in the ONL or inner nuclear layer (INL) from the same area of the histological sections.

Statistical analyses

Mann–Whitney U test was used to compare fluorescein staining scores between the exposed eye and control eye. The significance of differences in the amplitude ratio of ERG components between groups was evaluated by the one-factor ANOVA followed by Scheffe's F test. Fisher's least significant difference (LSD) test was performed to determine if the differences in the mean thickness of the outer nuclear layers between affected and control eyes were statistically significant. The differences were considered significant when $P < 0.05$.

Results

Spectral emission of flash unit

The spectral energy output from the photographic light bulb was measured with the spectroradiometer and plotted in Fig. 2. Emissions at wavelengths less than 380 nm were reduced significantly by the UV filter incorporated in the unit. However, a small amount of UV between 380 nm and 400 nm was transmitted through the filter, and a large amount of near-infrared radiant was emitted by the photographic flash lamp. The intensity of the light bulb was calculated to be 40 ± 2 J/m^2 ($n = 2$).

Fluorescein staining score

The mean ± standard deviation of the fluorescein score following the maximal light exposure

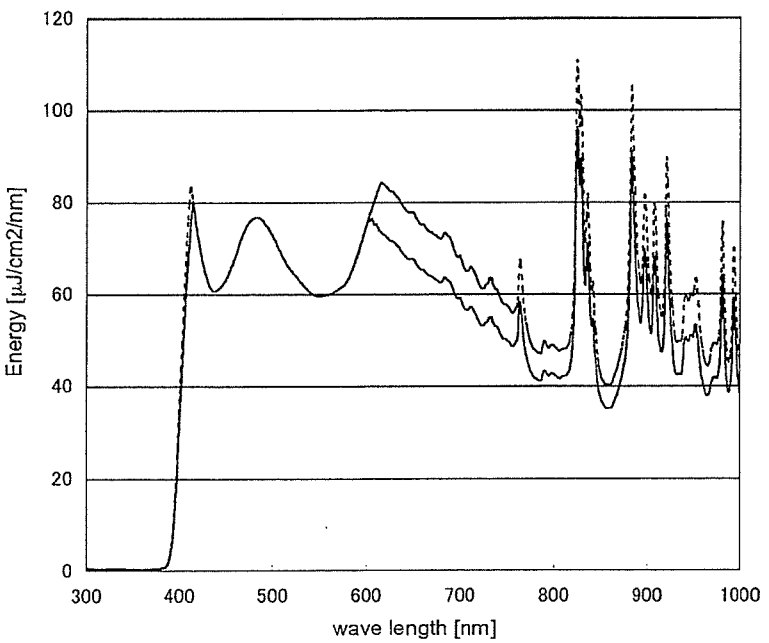

Fig. 2 Spectral emission of the light bulb. This bulb emits light throughout the visible spectrum and a UV filter is incorporated in the unit to attenuate wavelengths shorter than 380 nm

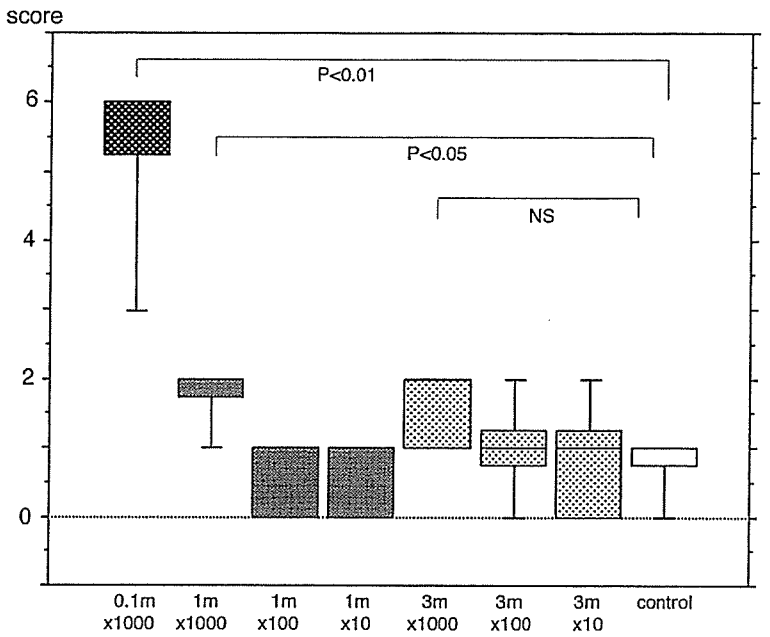

Fig. 3 Fluorescein staining score of the corneal epithelium 24 h after light exposure. The fluorescein scores after the maximum light exposure conditions (1,000 flashes at 0.1 m) and the exposure (1,000 flashes at 1 m) are significant higher than that of controls (P = 0.009, P = 0.028, the Mann–Whitney U test, respectively). Other exposures are not significantly different from that of controls (NS: not significant, box: Median ± 25 percentile, bar: range of actual measurement)

(1,000 flashes at 0.1 m) was 5.4 ± 0.9, which was significantly higher than that of control eyes (0.8 ± 0.4; P = 0.009, the Mann–Whitney U test, Fig. 3). The fluorescein scores for eyes set at 1 m (1.8 ± 0.4; P = 0.028, the Mann–Whitney U test) was also significantly higher but that at 3 m (1.6 ± 0.5; P = 0.076, the Mann–Whitney U test) was not significantly different from the scores of the control eyes. The fluorescein scores for eyes set at 1 m were 0.4 ± 0.5 after 10 flashes, and 0.6 ± 0.5 after 100 flashes, and the scores for eyes set at 3 m were 0.8 ± 0.8 after 10 flashes, 1.0 ± 0.7 after 100 flashes, and 1.6 ± 0.5 after 1,000 flashes. The fluorescein score increased as the number of flashes increased, but the increases in the scores were not significantly different from that of the control eyes.

The fluorescein score 7 days after the maximum light exposure (1,000 flashes at 0.1 m) had decreased to the control level of 0.6 ± 0.5 indicating a recovery of the corneal epithelium (n = 2). No cataract was seen by slit-lamp examination before and after any light exposure conditions.

Scanning electron microscopy (SEM)

Examinations of the corneas obtained after exposure to the maximum light conditions (1,000 flashes at 0.1 m) by SEM showed that many of the epithelial cells were detached from the surface of the cornea (Fig. 4). With less than 1,000 flashes or at farther distances of 3 m, no such changes were detected, and the hexagonal shapes of epithelial cells were well-preserved. The corneal epithelium recovered to the control level 7 days after the maximum light exposure (1,000 flashes at 0.1 m, n = 2).

Electroretinography (ERG)

The amplitude ratios (of after/before the light exposure) of the a-wave and b-wave were significant between groups (P = 0.0006, P = 0.0384, one factor ANOVA test, Figs. 5 and 6). In the eyes exposed to the maximum light level (1,000 flashes at 0.1 m), the mean ± standard deviation of the amplitude of the a-wave was significantly reduced by 23.0 ± 10.7% (P = 0.0026,

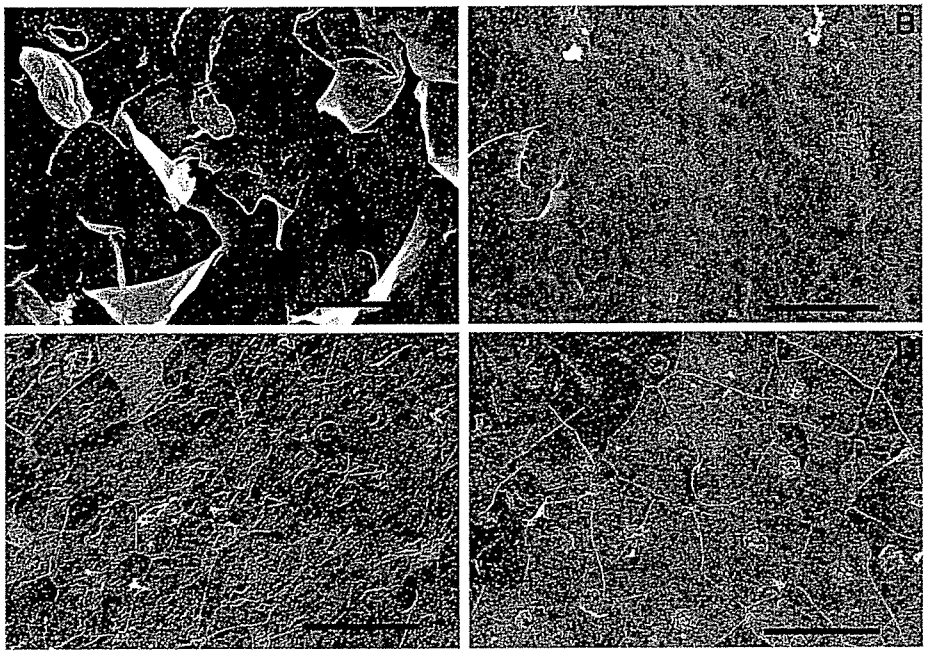

Fig. 4 Scanning electron photographs of cornea 24 h after light exposure. A: 1,000 flashes at 0.1 m. Edges of epithelial cells are detached from the surface of the cornea. B: 1,000 flashes at 1 m. No changes are seen. C: 1,000 flashes at 3 m. No changes are seen. D: control. No difference is observed at the longer distances (1 m or 3 m) even with the maximal number of flashes compared to the control (bar: 45 μm)

the Scheffe's F test) of that before the light exposure, but the amplitude in the eyes exposed at longer distances of 1 m or 3 m to 1,000 flashes was not reduced significantly (Figs. 5, 6A, $P > 0.9999$, $P = 0.9656$, respectively, the Scheffe's F test). The amplitude of the b-wave exposed to the maximum light level (1,000 flashes at 0.1 m) was also significantly reduced by 19.7 ± 7.0% (Figs. 5, 6B, $P = 0.0478$, the Scheffe's F test) of that before light exposure, but the amplitude in the eyes exposed at farther distances of 1 m or 3 m was not significantly reduced ($P = 0.8821$, $P = 0.6561$, respectively, the Scheffe's F test). The amplitude ratio of the control left eyes (no light exposure) was 100.4 ± 5.1% for the a-wave and 100.5 ± 6.7% for the b-wave. The amplitudes in a- and b-waves were not altered significantly following the other exposure levels.

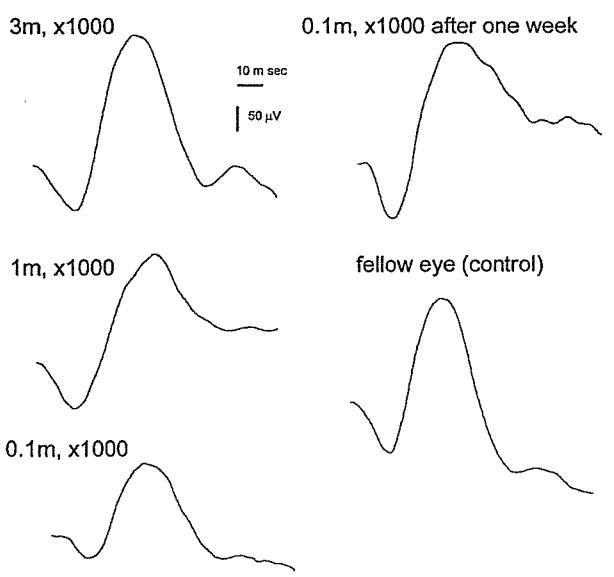

Fig. 5 Electroretinograms (ERGs) of rat eyes 24 h after the light exposure. The amplitudes of the a- and b-waves are reduced after the maximal light exposure (1,000 flashes at 0.1 m) but the amplitudes recover after 1 week

The amplitude of ERG components in the eyes exposed to the maximum light level recovered to 100.6 ± 13.3% for the a-wave and 100.8 ± 2.9% for the b-wave 1 week after the light exposure ($n = 2$).

Histopathological examination of retina

The mean thickness of the outer nuclear layers temporal and superior to the optic disc was 24 ± 1μm at 0.1 m with 1,000 flashes, 24 ± 2 μm at 1 m, 25 ± 2μm at 3 m and 24 ± 1μm in controls without light flashes (Fig. 7). These differences were not significant ($P = 0.92$ at 0.1 m, $P = 0.40$ at 1 m, $P = 0.45$ at 3 m, the LSD test). The architecture of the retina was not altered by any exposed level. The mean retinal thickness in the same area of the control eyes was 83 ± 6 μm, and the thickness in the same area was 86 ± 11 μm when the flash unit was set at 0.1 m and 1,000

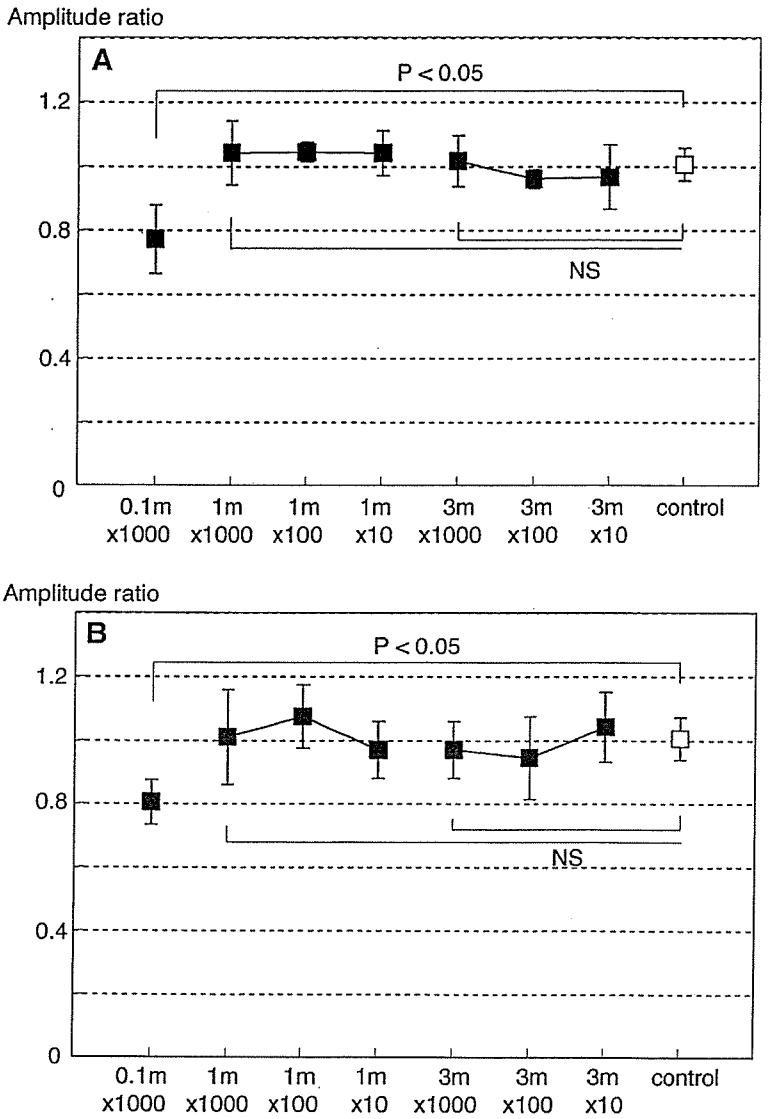

Fig. 6 The amplitude of the electroretinogram (ERG) of rat eyes 24 h after the light exposure. A: The amplitude of a-wave of the ERG following the maximum light exposure (1,000 flashes at 0.1 m) is reduced by 23.0% ± 10.7% ($P = 0.0026$, the Scheffe's F test) from the amplitude before the light exposure. No significant changes are seen following other levels of exposures. B: The amplitude of b-wave of the ERG following the maximum light exposure (1,000 flashes at 0.1 m) is reduced by 19.7% ± 7.0% ($P = 0.0478$, the Scheffe's F test) from the amplitude before the light exposure. No significant changes are seen following other levels of exposures (Amplitude ratio: the ratio of amplitude after the light exposure comparing before the exposure, NS: not significant, bar; mean ± standard deviation)

flashes were delivered. This difference was also not significant comparing with the control eyes ($P = 0.287$, the LSD test). Lower levels of light exposures also did not change the retinal thickness significantly (85 ± 7 μm at 1 m, $P = 0.591$, and 86 ± 14 μm at 3 m with 1,000 flashes, $P = 0.116$, the LSD test).

A significantly larger numbers of TUNEL positive cells were observed in the ONL of eyes exposed to the maximal light exposure (Fig. 8, $P = 0.02$, the LSD test). The ratio of the TUNEL positive cells to total cells was 0.52 ± 0.39% in the ONL in the eyes which had the maximal light exposure, while it was 0.03 ± 0.01% in the INL. With other light exposure conditions, none of the eyes showed more than 0.03% TUNEL positive cells in the ONL and the INL. No TUNEL positive cells were observed 1 week after the maximal light exposure.

Discussion

Damage of the ocular tissues in albino rats was produced only by the maximum exposure of the photoflash unit. This exposure exceeded that encountered in typical use of a flash photography unit. In addition, the damage was reversible. Excessive light exposure of the eye is known to damage the cornea, crystalline lens, retina, and retinal pigment epithelial cells [2, 3]. In the cornea, the damage is mainly of the epithelial cells which

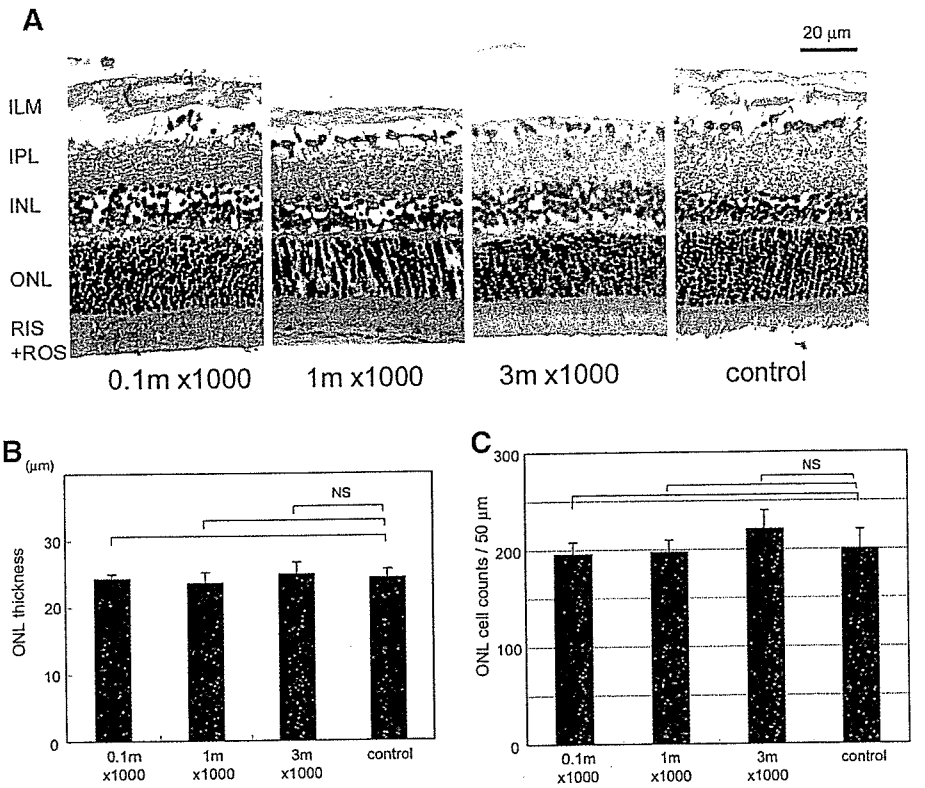

Fig. 7 Paraffin sections of posterior pole of the eyes 24 h after light exposure. A: Histological sections of posterior pole indicate no morphological damage in the retina of the eye for all levels of light exposure compared to the control eyes (Hematoxylin & eosin stain). B: The total retina thickness and C: the thickness of outer nuclear layer (ONL) 24 h after 1,000 flashes in each distance are not significant to those of control eyes

are detached from the surface of the cornea, and this change is caused by the light from the UV-end of the spectrum [4]. Although the flash unit used in this experiment is equipped with a UV filter that greatly attenuates wavelengths shorter than 380 nm, our findings showed that sufficient UV energy was still transmitted to the cornea to cause the detachment of some of the epithelial cells.

Chronic light exposure can lead to photochemical alterations to the lens which also results from the absorption of UV-A light to cause nuclear cataracts [2]. Intensive laser irradiation can cause heat-derived lens opacification in the patients with cataracts, but visible light, such as that emitted from photographic flash units for a short duration is unlikely to cause serious damage to the crystalline lens.

Light damage to the retina has been shown to result from either thermal or photochemical effects. From the studies of Noell and colleagues, the photochemical effect is most likely the major factor involved in the retinal light damage [12].

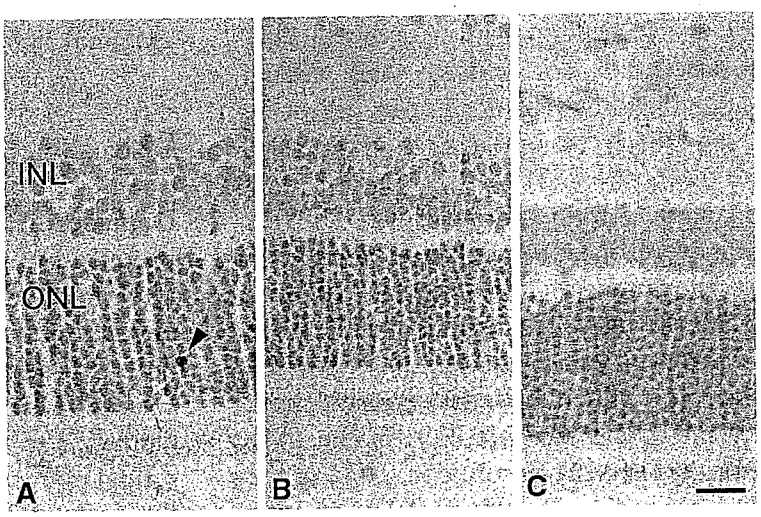

Fig. 8 Apoptosis following light exposure in the posterior pole of the eyes 24 h after light exposure. A: 0.1 m × 1,000 flashes. B: 1 m × 1,000 flashes. C: 3 m × 1,000 flashes. TUNEL-positive cells (arrow head) are seen in outer nuclear layer (ONL), indicating apoptosis of the photoreceptorcells following the maximal exposure but no positive cells in other conditions (bar: 20 μm)

The thermal effects result from an increase in temperature caused by the absorption of light energy by the melanin pigments in the RPE and choriod [12]. Blue light irradiation, on the other hand, leads to a minimal increase in temperature, but the threshold of blue light energy necessary to cause tissue damage was estimated to be <0.001 of that of infrared irradiance [13]. Thus, these characteristics indicate that the photochemical effect played a major role in the retinal damage caused by visible light.

The mechanism for the damage has been suggested to arise from the production of phototoxic substances by the partially transmitted UV-light or blue light from the flash lamp. On the other hand, high tissue temperatures can enhance tissue damage and low temperatures minimize the damage [14, 15]. Thus, the near-infrared radiant component in the photographic flash light may enhance tissue damage. However, the synthesis of heat-shock proteins induced by a brief, whole body hyperthermic treatment has been shown to be protective by enhancing photoreceptor cell survival against light damage [16, 17].

Reductions in the amplitude of the ERGs has been reported to indicate retinal light damage and is correlated with the degree of retinal damage [18–22]. Our results showed that the ERGs recorded from the eyes exposed to the maximum light levels were reduced at 24 h after exposure, but they recovered to normal values after 1 week. These transient decreases of ERG amplitude may reflect physiologically a consumption of the outer segments of the photoreceptors without significant histological degeneration of the ONL and the outer segments may have been renewed within a week.

Retinal light damage has also been investigated histologically [22–25]. Blue light damage was reported to cause depigmentation of the retinal pigment epithelium, while near UV light caused tissue damage in the outer segments in addition to the RPE damage [25]. These wavelengths are thought to induce oxidative stress after their absorption in the tissue [26, 27]. In our study, histological examinations did not reveal any major damage in retinal architecture with no significant change in retinal thickness. However, a significant increase in the number of TUNEL-positive apoptotic nuclei was observed in the outer nuclear layer after the maximal light exposure. TUNEL positive cells have been reported to be present in the outer nuclear layer after photic injury to the rat retina [28, 29]. Intense light exposure can induce apoptotic changes in many photoreceptor cells even after a short exposure, and this would suggest that the photoreceptor cell death starts immediately after the exposure [29]. However, the percentage of TUNEL-positive apoptotic cells were only 0.52% even after the maximal exposure which should then not affect the total retinal cell structure to decrease the retinal thickness in the ONL.

Our results showed that the light exposure of the photographic flash unit can cause transient corneal epithelial cell damage and transient impairment in retinal function. It is suggested that the threshold for corneal and retinal damage may lie between the maximum exposure and the next highest. However, this maximal exposure condition is very unusual. An exposure of 1,000 flashes at 0.1 m corresponds to approximate 100,000 flashes at 1 m in total light energy if the distance of 1 m can be considered to be the one used in normal situations. Therefore, we conclude that the phototoxic effect of this commercially available photographic flash unit is minimal to the cornea and retina when used in an appropriate way.

Acknowledgements This study was supported by the research grant by Fuji Film Corporation, Tokyo, Japan. The authors would like to acknowledge the technical assistance of T. Nagai with electron microscopy.

References

1. Wasowicz M, Morice C, Ferrari P, et al (2002) Long-term effects of light damage on the retina of albino and pigmented rats. Invest Ophthalmol Vis Sci 43:813–820
2. Zrenner E (1990) Light-induced damage to the eye. Fortschr Ophthalmol 87(suppl):S41–S51
3. Roberts JE (2001) Ocular phototoxicity. J Photochem Photobiol B 64:136–143
4. Podskochy A, Gan L, Fagerholm P (2000) Apoptosis in UV-exposed rabbit corneas. Cornea 19:99–103
5. Jaffe GJ, Irvine AR, Wood IS, et al (1988) Retinal phototoxicity from the operating microscope. The role of inspired oxygen. Ophthalmology 95:1130–1141

6. Tso MOM, Woodford BJ (1983) Effect of photic injury on the retinal tissues. Ophthalmology 90: 952–963
7. Ross WH (1984) Light-induced maculopathy. Am J Ophthalmol 98:488–493
8. van den Bissen PR, Berenschot T, Verdaasdonk RM, et al (2000) Endoillumination during vitrectomy and phototoxicity thresholds. Br J Ophthalmol 84: 1372–1375
9. Zamir E, Kaiserman I, Chowers I (1999) Laser pointer maculopathy. Am J Ophthalmol 127:728–729
10. Noell WK (1980) There are different kinds of retinal light damage in the rat. In: Williams TP, Baker BN (eds) The effect of constant light on visual processes. Plenum Press, New York, pp 3–28
11. Rapp LM, Williams TP (1980) A parametric study of retinal light damage in albino and pigmented rats. In: Williams TP, Baker BN (eds) The effect of constant light on visual processes. Plenum Press, New York, pp 135–159
12. Noell WK, Walker VS, Kang BS, Berman S (1966) Retinal damage by light in rats. Invest Ophthalmol 5:450–473
13. Ham WT Jr, Meuller HA, Slinery DH (1976) Retinal sensitivity to damage from short wavelength light. Nature 260:153–155
14. Mori K, Yoneya S, Hayashi N, Abe T (1997) Fundus hypothermia inhibits retinal damage induced by visible blue light. Nippon Ganka Gakkai Zasshi 101:633–638
15. Organisciak DT, Darrow RM, Nell WK, Blanks JC (1995) Hyperthermia accelerates retinal light damage in rats. Invest Ophthalmol Vis Sci 36:997–1008
16. Barbe MF, Tytell M, Gower DJ, Welch WJ (1988) Hyperthermia protects against light damage in the rat retina. Science 241:1817–1820
17. Tytell M, Barbe MF, Brown IR (1994) Induction of heat shock (stress) protein 70 and its mRNA in the normal and light-damaged rat retina after whole body hyperthermia. J Neurosci Res 38:19–31
18. Sugawara T (2002) Electroretinogram changes in eyes with light damage to the retina. Folia Ophthalmol Jpn 53:609–615
19. Ohuchi T, Machida S, Tazawa Y (1994) Changes in ERG a, b and c-waves by light-induced retinal damage. Folia Ophthalmol Jpn 45:952–955
20. Kartz KE, Newsome DA, May JG (1990) Changes in ERG amplitude following laser induced damage to the primate retina. Curr Eye Res 9:435–444
21. Sugawara T, Sieving PA, Bush RA (2000) Quantitative relationship of the scotopic and photopic ERG to photoreceptor cell loss in light damaged rats. Exp Eye Res 70:693–705
22. Takahashi T, Machida S, Masuda T, et al (2005) Functional changes in rod and cone pathways after photoreceptor loss in light-damaged rats. Curr Eye Res 30:703–713
23. Kozaki J, Takeuchi M, Takahashi K, et al (1994) Light-induced retinal damage in pigmented rabbit-1 histopathological observations of the natural course of healing. Nippon Ganka Gakkai Zasshi 98:738–748
24. Ham WT Jr, Mueller HA, Ruffolo JJ Jr, et al (1982) Action specrum for retinal injury from near-ultraviolet radiation in the aphakic monkey. Am J Ophthalmol 93:229–306
25. Busch EM, Gorgels TG, van Norren D (1999) Temporal sequence of changes in rat retina after UV-A and blue light exposure. Vision Res 39:1233–1247
26. Ham WT Jr, Mueller HA, Ruffolo JJ Jr, et al (1984) Basic mechanisms underlying the production of photochemical lesions in the mammalian retina. Curr Eye Res 26:165–174
27. Wang L, Lam TT, Lam KW, Tso MO (1984) Correelation of phospholipids hydroperoxidase glutathione peroxidase activity to the sensitivity of rat retinas to photic injury. Ophthalmic Res 26:60–64
28. Aonuma H, Yamazaki R, Watanabe I (1999) Retinal cell death by light damage. Jpn J Ophthalmol 43:171–179
29. Shahinfar S, Edward DP, Tso MO (1991) A pathologic study of photoreceptor cell death in retinal photic injury. Curr Eye Res 10:47–59

PNAS
Proceedings of the National Academy of Sciences of the United States of America www.pnas.org

Drusen, choroidal neovascularization, and retinal pigment epithelium dysfunction in SOD1-deficient mice: A model of age-related macular degeneration

Yutaka Imamura, Setsuko Noda, Kouhei Hashizume, Kei Shinoda, Mineko Yamaguchi, Satoshi Uchiyama, Takahiko Shimizu, Yutaka Mizushima, Takuji Shirasawa, and Kazuo Tsubota

PNAS 2006;103;11282-11287; originally published online Jul 14, 2006;
doi:10.1073/pnas.0602131103

Drusen, choroidal neovascularization, and retinal pigment epithelium dysfunction in SOD1-deficient mice: A model of age-related macular degeneration

Yutaka Imamura*†, Setsuko Noda‡, Kouhei Hashizume*, Kei Shinoda*§, Mineko Yamaguchi¶, Satoshi Uchiyama¶, Takahiko Shimizu¶, Yutaka Mizushima‖, Takuji Shirasawa¶, and Kazuo Tsubota*†**

*Department of Ophthalmology, Keio University School of Medicine, 35-Shinanomachi, Shinjuku-ku, Tokyo 160-8582, Japan; ‡Department of Nursing, Tokai University School of Health Science, Boseidai, Isehara, Kanagawa 259-1193, Japan; §Laboratory of Visual Physiology, National Institute of Sensory Organs, National Hospital Organization, Tokyo Medical Center, 2-5-1-Higashigaoka, Meguro-ku, Tokyo 152-8902, Japan; ¶Research Team for Molecular Biomarkers, Tokyo Metropolitan Institute of Gerontology, Itabashi-ku, Tokyo 173-0015, Japan; ‖DDS Institute, Jikei University School of Medicine, 3-25-8 Nishi-shinbashi, Minato-ku, Tokyo 105-8461, Japan; and **Department of Ophthalmology, Tokyo Dental College, 5-11-13 Sugano, Ichikawa, Chiba 272-8513, Japan

Edited by Jeremy Nathans, Johns Hopkins University School of Medicine, Baltimore, MD, and approved June 9, 2006 (received for review March 19, 2006)

Oxidative stress has long been linked to the pathogenesis of neurodegenerative diseases; however, whether it is a cause or merely a consequence of the degenerative process is still unknown. We show that mice deficient in Cu, Zn-superoxide dismutase (SOD1) have features typical of age-related macular degeneration in humans. Investigations of senescent *Sod1*$^{-/-}$ mice of different ages showed that the older animals had drusen, thickened Bruch's membrane, and choroidal neovascularization. The number of drusen increased with age, and exposure of young *Sod1*$^{-/-}$ mice to excess light induced drusen. The retinal pigment epithelial cells of *Sod1*$^{-/-}$ mice showed oxidative damage, and their β-catenin-mediated cellular integrity was disrupted, suggesting that oxidative stress may affect the junctional proteins necessary for the barrier integrity of the retinal pigment epithelium. These observations strongly suggest that oxidative stress may play a causative role in age-related retinal degeneration, and our findings provide evidence for the free radical theory of aging. In addition, these results demonstrate that the *Sod1*$^{-/-}$ mouse is a valuable animal model to study human age-related macular degeneration.

animal model | superoxide dismutase

Age-related macular degeneration (AMD) is the leading cause of legal blindness in humans in developed countries (1–5). AMD is characterized by a progressive degeneration of the macula, usually bilateral, leading to a severe decrease in vision and a central scotoma. The decrease in vision results either from retinal degeneration, called geographic atrophy (dry or nonexudative AMD), or from the secondary effects of choroidal neovascularization (CNV; wet or exudative AMD). An early sign of AMD is the appearance of drusen, which are extracellular deposits that accumulate below the retinal pigment epithelium (RPE) and are known to be risk factors for developing CNV (6–8).

Mouse models of AMD that manifest some of the features of human AMD have recently begun to appear (9–14); however, most of these mice have only some of the characteristics of human AMD (15). The severity of AMD in humans progresses with increasing age, finally resulting in extensive degeneration of the retina. Therefore, animal models that mimic the complex and progressive characteristics of AMD are needed to investigate the pathogenesis of AMD.

Oxidative stress, which refers to cellular or molecular damage caused by reactive oxygen species (ROS), has been implicated in many age-related diseases and aging itself (16, 17). ROS include free radicals, hydrogen peroxide, and singlet oxygen and are often the by-products of oxygen metabolism. The retina is particularly susceptible to oxidative stress because of its high consumption of oxygen, high concentration of polyunsaturated fatty acids, and exposure to light (18). A growing body of evidence suggests that cumulative oxidative damage may be responsible for AMD (18, 19); however, a causative link has not been definitively demonstrated (18).

To determine whether there is a causative role of oxidative stress in the pathogenesis of AMD, we first focused on the age-related changes in the eyes of mice deficient in oxidative stress scavengers. One of the main antioxidant systems in the retina is made up of three superoxide dismutase (SOD) isoenzymes that catalyze superoxide radical dismutation (20). Cu, Zn-SOD (SOD1) exists in the cytosol, Mn-SOD (SOD2) in the mitochondrial matrix, and extracellular SOD (SOD3) in the tissue interstitium as the secretory form (21). Because the amount and activity of SOD1 are highest among the three isoenzymes in the human retina (21), it seemed reasonable to hypothesize that the lack of SOD1 would accelerate age-related pathological changes in the human retina.

We have investigated the age-related changes of the retinas of *Sod1*$^{-/-}$ mice and found that these mice have many of the key elements of human AMD including drusen, thickened Bruch's membrane, and CNV. Moreover, the RPE cells of these mice show signs of oxidative damage, and their junctional integrities are damaged with the disruption of β-catenin-mediated cell adhesions. Thus, our results suggest a causative role of oxidative stress in the pathogenesis of retinal degeneration and demonstrate the critical role of SOD1 in protecting the RPE from age-related degeneration.

Results

Drusen in Senescent *Sod1*$^{-/-}$ Mice. Fundus examinations were performed on 60 *Sod1*$^{-/-}$ mice (age, 3–18 months) and 50 age-matched wild-type mice. The fundi of *Sod1*$^{-/-}$ mice ($n = 25$) under 7 months of age appeared normal and indistinguishable from those of wild-type mice ($n = 25$). Mice older than 7 months showed white to slightly yellowish retinal deposits that appeared to be similar to drusen in humans (Fig. 1*A*). The drusen were hyperfluorescent during fluorescein angiography, as in humans (Fig. 1*B*), and the numbers increased with age (Fig. 1*C*). Drusen were detected in 31 of 36 eyes (86%) of *Sod1*$^{-/-}$ mice older than 10 months. In contrast, wild-type mice and heterozygous mice

Conflict of interest statement: No conflicts declared.

This paper was submitted directly (Track II) to the PNAS office.

Freely available online through the PNAS open access option.

Abbreviations: AMD, age-related macular degeneration; CNV, choroidal neovascularization; RPE, retinal pigment epithelium; SOD, superoxide dismutase; C5, complement 5; CML, carboxymethyl lysine.

†To whom correspondence may be addressed. E-mail: imamura@sc.itc.keio.ac.jp or tsubota@sc.itc.keio.ac.jp.

www.pnas.org/cgi/doi/10.1073/pnas.0602131103

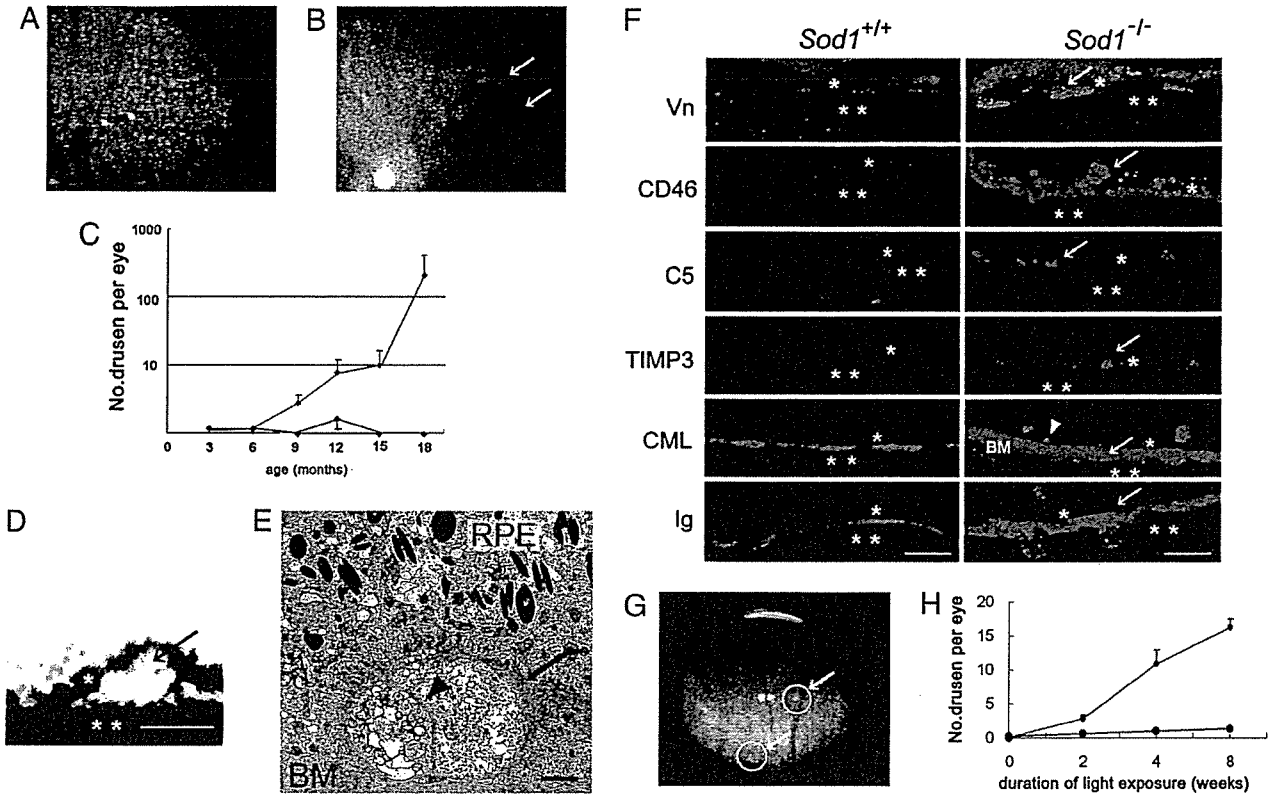

Fig. 1. Senescent *Sod1*$^{-/-}$ mice showing drusen. (*A*) Fundus photograph from a 15-month-old *Sod1*$^{-/-}$ mouse. White and slightly yellowish deposits are evident (arrows). (*B*) Fluorescein angiogram showing hyperfluorescent areas corresponding to the sites of the drusen (arrows). (*C*) Plot of the number of drusen in *Sod1*$^{-/-}$ mice at 3–18 months of age, showing an increase in the number of drusen with age. Values for *Sod1*$^{-/-}$ are plotted in red, and those for *Sod1*$^{+/+}$ are plotted in blue. (*D*) Dome-shaped deposit (arrow) between the RPE (*) and choroid (**) in a 12-month-old *Sod1*$^{-/-}$ mouse. (*E*) Electron micrograph of drusen (arrow) from a 12-month-old *Sod1*$^{-/-}$ mouse. Heterogeneous materials separated by a septum (arrowhead) are observed. The drusen appears to contain debris-like material of outer segments. BM, Bruch's membrane. (*F*) Immunohistochemistry with markers for vitronectin (Vn), CD46, C5, TIMP3, CML, and Ig. Drusen and/or their surrounding tissues from 12-month-old *Sod1*$^{-/-}$ mice (*Right*) are positive for vitronectin, CD46, C5, TIMP3, CML, and Ig in contrast to the results for age-matched wild-type mice (*Left*). *, RPE; **, choroid; arrow, positive signal; arrowhead, positive signal of CML in RPE cell layer. (*G*) Fundus changes in a 5-month-old *Sod1*$^{-/-}$ mouse after continuous light exposure for 8 weeks (white fluorescent light of 10,000 lux). Drusen are present (circles and arrows). (*H*) The number of drusen increases with the length of light exposure in *Sod1*$^{-/-}$ mice, as compared with the minimal appearance of drusen in wild-type mice. Values for *Sod1*$^{-/-}$ are plotted in red, and those for *Sod1*$^{+/+}$ are plotted in blue. (Scale bars: *D* and *F*, 50 μm; *E*, 2 μm.)

(*Sod1*$^{+/-}$) showed very few, if any, drusen (Figs. 2*A* and 3 *A*, *C*, and *E*).

Light microscopic examination of histological sections of the retinas of a 12-month-old *Sod1*$^{-/-}$ mouse showed dome-shaped deposits between the RPE and Bruch's membrane (Fig. 1*D*). Heterogeneous materials were detected beneath the RPE on Bruch's membrane by electron microscopy (Fig. 1*E*).

Markers of drusen, including vitronectin, a fluid-phase regulator binding the terminal component complex to regulate the control complex-mediated lysis (22); CD46, a membrane-bound regulator that facilitates inactivation of activated complement components (23); complement 5 (C5); tissue inhibitor of metalloproteinases 3 (TIMP3), a potent local inhibitor of matrix metalloproteinase regulating the rate of Bruch's membrane turnover (24); carboxymethyl lysine (CML); and Igs were detected in the drusen by immunohistochemistry (Fig. 1*F*).

In a proteomics analysis by Crabb *et al.* (25), vitronectin, TIMP3, and CML were found in the drusen of human cadaver eyes with AMD. In the retinas of *Sod1*$^{-/-}$ mice, positive staining for CD46, C5, and Ig was observed to extend beyond the RPE, which would indicate that the inflammatory reactions occurred, not only at the site of the drusen, but also in the surrounding tissues, including the retina (Fig. 1*F*). These findings are consistent with recent findings that local inflammation involving Igs, complements, and complement-related genes may play a role in the pathogenesis of AMD in humans (26–29).

Induction of Drusen by Exposure to Light. Because exposure to light (30, 31) and smoking (32) have been reported in epidemiological studies to be risk factors for AMD in humans, we attempted to induce drusen in young *Sod1*$^{-/-}$ mice by light exposure. Young *Sod1*$^{-/-}$ mice (age, 5 months) have normal retinal architecture and do not have any drusen. However, after constant white fluorescent light exposure (10,000 lux, equal to outdoor sunlight) for 24 h per day, drusen appeared (Fig. 1*G*), and their numbers increased with the duration of the light exposure (Fig. 1*H*)

Degeneration of RPE and Thickened Bruch's Membrane in *Sod1*$^{-/-}$ Mice. Degenerative changes of the RPE and photoreceptor cell layer are another hallmark of both the wet and dry types of AMD in humans (33). Degeneration of the RPE was observed in a 12-month-old *Sod1*$^{-/-}$ mouse by electron microscopy (Fig. 2 *A* and *B*). Bruch's membrane was markedly thickened (Fig. 2*A* and *B*) with vacuolization of the RPE cells (Fig. 2*B*, asterisk) in a 12-month-old *Sod1*$^{-/-}$ mouse. The mean thickness of Bruch's membrane in the eyes of 10- to 12-month-old *Sod1*$^{-/-}$ mice (n = 4) was 3.2 ± 1.5 μm in contrast to that in the wild-type (n = 4, 0.5 ± 0.2 μm, $P < 0.05$). Loss of the photoreceptor cell was also

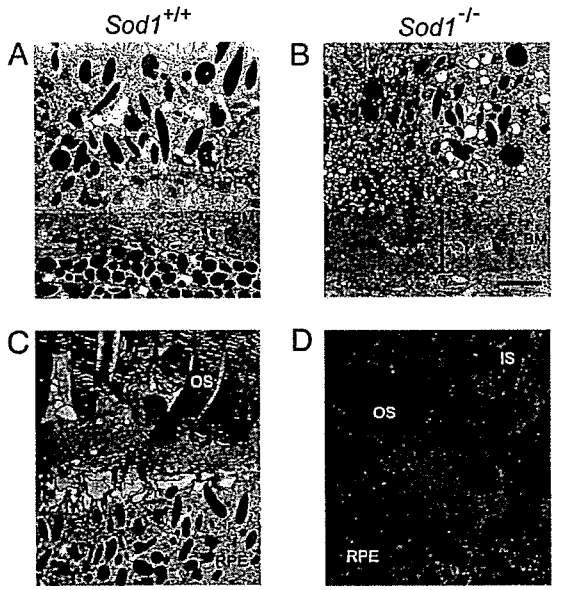

Fig. 2. Degenerated RPE and thickened Bruch's membrane in *Sod1*$^{-/-}$ mice. (*A*) Ultrastructure of Bruch's membrane (BM) in a 12-month-old wild-type mouse. (*B*) Thickened Bruch's membrane of an age-matched *Sod1*$^{-/-}$ mouse. RPE cells show marked vacuolization (*). (*C*) Ultrastructure of the outer segments (OS) of the photoreceptor cells and RPE of a 12-month-old wild-type mouse. (*D*) Destruction of inner segments (IS), outer segments, and RPE in an age-matched *Sod1*$^{-/-}$ mouse. (Scale bars: *B* and *D*, 2 μm.)

detected in 5 of 30 *Sod1*$^{-/-}$ mice (17%) that were examined histologically (representative case shown in Fig. 2 *C* and *D*). These alterations are consistent with histopathological findings in human eyes with AMD (33).

CNV in *Sod1*$^{-/-}$ Mice. The presence of CNV is a hallmark of the wet type of AMD in which the neovascularization in the choroid extends into the RPE and subretinal space. We found that 5 of 60 *Sod1*$^{-/-}$ mice (8.3%) showed an exudative lesion by fundus examination (Fig. 3 *A* and *B*), and 3 of 30 *Sod1*$^{-/-}$ mice older than 10 months (10%) had CNV by histological examination. The CNVs were confirmed by dye leakage during fluorescein angiography (Fig. 3 *C* and *D*). In contrast, the wild-type mice did not show CNV by fundus examination (n = 50) or histological examinations (n = 30).

Histological examination of the retinal sections containing the exudative lesion seen by ophthalmoscopy and area of dye leakage showed intraretinal fibrovascular tissues extending from the choroid into the retina (Fig. 3 *E* and *F*). In a 15-month-old *Sod1*$^{-/-}$ mouse, the CNV beneath the RPE can be seen to penetrate through Bruch's membrane, and the blood vessel cavity was surrounded by cells positive for CD31, a marker for endothelial cells (Fig. 3*G*). A 16-month-old senescent *Sod1*$^{-/-}$ mouse had CNV penetrating into the sensory retina (Fig. 3*H*). Electron microscopy showed ruptures of the Bruch's membrane and the RPE cell layer at the site of the CNV (Fig. 3*I*).

Oxidative Damage of RPE and Disruption of β-Catenin-Mediated Cellular Integrity of RPE in *Sod1*$^{-/-}$ Mice. Western blot analysis showed a lack of expression of SOD1 protein in the eyes of *Sod1*$^{-/-}$ mice (n = 3). The expressions of SOD2 and SOD3 proteins in *Sod1*$^{-/-}$ mice did not differ significantly from those in wild-type mice (Fig. 4*A*). Histochemical analysis showed the diffuse expression of SOD1 in all layers of retina of wild-type mice and the complete absence in *Sod1*$^{-/-}$ mice, in contrast to its presence in SOD2 mice (Fig. 4*B*).

A marker of oxidative damage to DNA (34), 8-hydroxy-2′-deoxyguanosine (8-OHdG), was detected in the RPE of *Sod1*$^{-/-}$ mice but was minimally present in wild-type mice (Fig. 5*A*). CML, a marker of oxidative protein modification (35), was deposited in the thickened Bruch's membrane (Fig. 1*F*) and RPE (Fig. 1*F*, arrowhead) in *Sod1*$^{-/-}$ mice, suggesting that the RPE and surrounding tissues had been damaged by oxidative processes in *Sod1*$^{-/-}$ mice.

To determine the effect of oxidative stress on the RPE, we examined whether the adherence junction proteins, which make up the barrier integrity of the RPE, were present in *Sod1*$^{-/-}$ mice (36). The location of β-catenin in the RPE of senescent *Sod1*$^{-/-}$ mice was studied in flat-mount preparations of the RPE. The presence of β-catenin was incomplete in the periphery of the RPE, indicating a disruption of the junctional integrity of the RPE (Fig. 5*B*, arrows) that is consistent with the light and electron microscopic observations (Figs. 1*D*, 2*B*, and 3 *F* and *I*). The cytoplasmic level of β-catenin was higher in the RPE cells of a 10-month-old *Sod1*$^{-/-}$ mouse than in a wild-type mouse (Fig. 5*C*). Quantitative measurement of the cytoplasmic β-catenin level of the RPE cells of 12-month-old *Sod1*$^{-/-}$ mice and age-matched wild-type mice (n = 49, each group) revealed a 63.3% increase in the cytoplasmic level in the *Sod1*$^{-/-}$ mice (Fig. 5*E*, $P < 0.001$). These results are compatible with an *in vitro* study showing that oxidative stress changes the cellular distribution of β-catenin and that the cytoplasmic level of β-catenin increased after the exposure of hydroxyl peroxide in ARPE-19 cells, a human RPE cell line (36).

The distribution of N-cadherin was also altered in the RPE of *Sod1*$^{-/-}$ mice (Fig. 5*D*). The expression of junction adherence proteins, including β-catenin and N-cadherin, is necessary to maintain an epithelial phenotype. Increased cytoplasmic levels of β-catenin were observed in the RPE cells of *Sod1*$^{-/-}$ mice *in vivo*, suggesting that chronic oxidative damage to the RPE may change the location of β-catenin from cell walls to cytoplasm, which then leads to the destruction of cell junctions maintained by the cadherin–catenin complex.

Because RPE damage promotes CNV growth, oxidative stress to the RPE and the disruption of β-catenin-mediated integrity may possibly be one of the initial events in this AMD model.

Discussion

Our results indicated that the retinas of senescent *Sod1*$^{-/-}$ mice have many features of the retinas of patients with AMD and recapitulated well the key elements of the human pathology. We demonstrated that drusen accumulated with increasing age in these mice, and histological examination revealed that the appearance of the drusen was quite similar to those in humans. We also showed that the major components of human drusen were present in the drusen of *Sod1*$^{-/-}$ mice and that drusen could be induced in young *Sod1*$^{-/-}$ mice by exposure to light. These findings strongly suggest that oxidative stress plays a causative role in initiating drusen formation.

Current animal models of CNV mostly use laser injury to fracture Bruch's membrane (37) or use viral transfection of angiogenic factors into RPE cells to induce CNVs (38). In our model, we used mice deficient in SOD1. The CNVs in our mice penetrated Bruch's membrane, and fluorescein angiography showed that the CNVs had a spiraling pathway into the sensory retina.

Recently, it was reported that mice deficient in *Ccl2*$^{-/-}$ or *Ccr2*$^{-/-}$ had angiogenic leakage, implying that macrophage dysfunction can induce CNV (10). These mice had retinal degeneration and drusen-like structures that increased in number with age (10). Several other mouse models of AMD have been reported. However, according to the most recent review (15), only the *Ccl2*$^{-/-}$, *Ccr2*$^{-/-}$, and *Sod1*$^{-/-}$ mice have the characteristics of both drusen and CNV. Moreover, drusen can

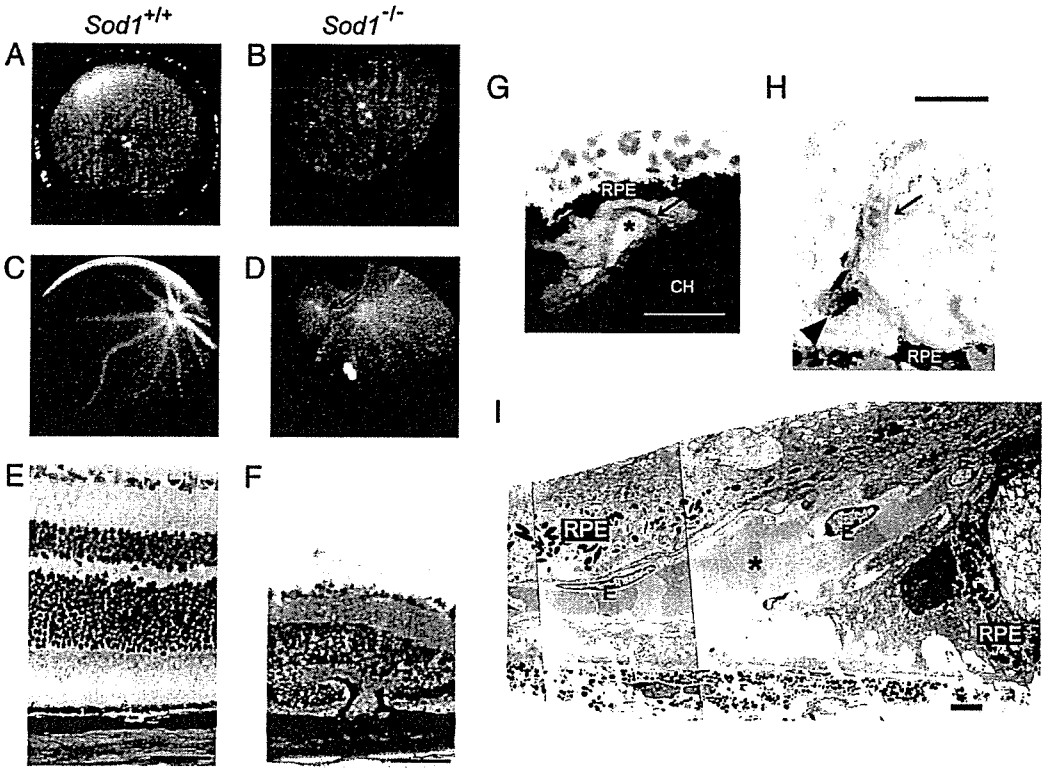

Fig. 3. CNVs in *Sod1*$^{-/-}$ mice. (*A*) Fundus of a 15-month-old wild-type mouse. (*B*) Fundus of a 15-month-old *Sod1*$^{-/-}$ mouse showing exudative retinal changes (arrow) adjacent to the optic disk. (*C*) Fluorescein angiogram of the wild-type mouse reveals no abnormal findings. (*D*) Fluorescein angiogram reveals dye leakage (arrow) from the CNV in a 15-month-old *Sod1*$^{-/-}$ mouse. (*E*) Hematoxylin and eosin staining of a retinal section of a wild-type mouse. (*F*) Fibrovascular tissue (arrow) involving RPE in the thinned retina of the *Sod1*$^{-/-}$ mouse. A thinning of the outer nuclear layer can be seen. Hematoxylin and eosin staining. (*G*) CNV in a 12-month-old *Sod1*$^{-/-}$ mouse. CNV is present beneath the RPE, and the vascular cavity (*) is surrounded by CD31-positive (diaminobenzidine) endothelial cells (arrow). Methyl green counterstaining was used. CH, choroid. (*H*) CNV with vessel cavity filled with erythrocytes (arrow) proliferates spirally into the sensory retina in a 12-month-old *Sod1*$^{-/-}$ mouse. RPE is attached within the intraretinal vascular structure (arrowhead). Toludine blue was used for staining. (*I*) Electron micrograph of CNV. CNV (*) surrounded by endothelial cells (E) pass through a defect in Bruch's membrane. RPE is severely disrupted. (Scale bars: *E–H*, 50 μm; *I*, 2 μm.)

be induced by photooxidative stress in *Sod1*$^{-/-}$ mice, which seems to be compatible with the clinical finding that subjects with a longer duration of sunlight exposure are more susceptible to soft drusen (30). Because retinal degeneration after constant light exposure was similar in the wild-type and *Sod1*$^{-/-}$ mice (data not shown), the accumulation of drusen seems to be due to the increased oxidative stress to the RPE rather than to the photoreceptors.

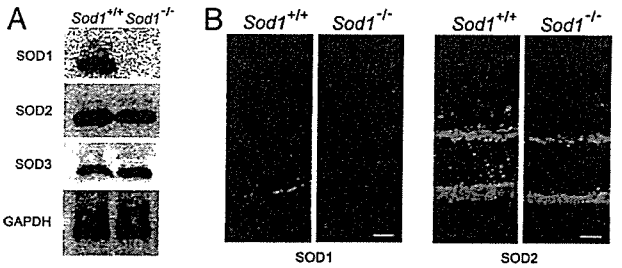

Fig. 4. Expression of SOD1, SOD2, and SOD3 in the eyes of *Sod1*$^{-/-}$ mice. (*A*) Western blot analysis reveals the absence of SOD1 protein expression in the eyes of *Sod1*$^{-/-}$ mice. The protein levels of SOD2 (Mn-SOD) and SOD3 (extracellular SOD) appear to be the same in wild-type and *Sod1*$^{-/-}$ mice. (*B*) SOD1 and SOD2 expression in the retinas of wild-type and *Sod1*$^{-/-}$ mice. (Scale bars: 50 μm.)

Our results demonstrated that complex phenotypes similar to those of human AMD can be caused by deficiency of a single gene, and the movement of β-catenin to the cytoplasm may explain the destruction of the cellular integrity of RPE. This would then contribute to the formation of drusen and CNV. Because the SOD2 and SOD3 proteins are still present in *Sod1*$^{-/-}$ mice, SOD1 as a cytoplasmic scavenger of reactive oxygen species (ROS) may play a major role in protecting RPE cells from oxidative damages.

As in other neurodegenerative disorders of the CNS, the pathogenesis of human AMD has long been linked to oxidative stress, although its causative role has not been definitively determined. Indirect evidence that oxidative damage is associated with AMD comes from epidemiological studies showing that smoking and sunlight exposure significantly increase the risk of AMD (30–32). In addition, supplementation with antioxidants including vitamin C, vitamin E, β-carotene, copper, and zinc can slow the progression of the disease (39).

SOD1 is an abundant copper- and zinc-containing protein present in the cytosol, nucleus, peroxisomes, and mitochondrial intermembrane space. Its primary function is to act as an antioxidant enzyme, lowering the steady-state concentration of superoxide (20). Therefore, our results strongly suggest that oxidative stress is not merely an associated phenomenon but a primary cause of age-related retinal degeneration.

The relationship between SOD and AMD has been studied in humans. However, the activity of SOD in erythrocytes has not

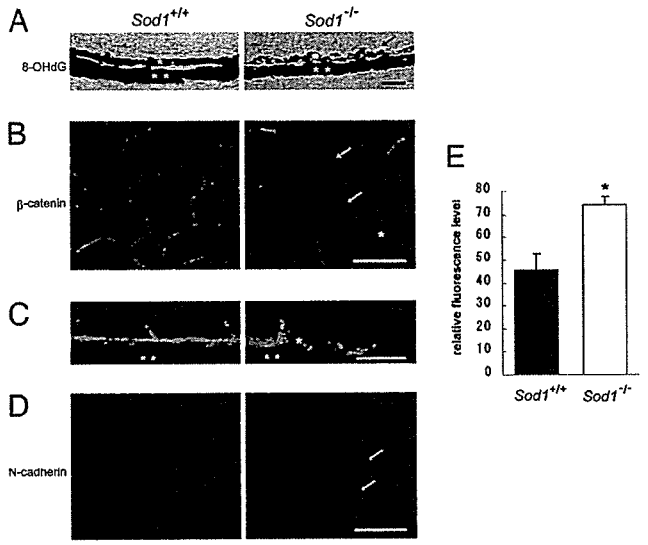

Fig. 5. Oxidatively damaged RPE and its disrupted β-catenin-mediated integrity in $Sod1^{-/-}$ mice. (*A*) 8-hydroxy-2′-deoxyguanosine (8-OHdG) was minimally present in the RPE of a 10-month-old wild-type mouse; however, it is markedly up-regulated in the RPE of a 10-month-old $Sod1^{-/-}$ mouse (arrow). *, RPE; **, choroid. (*B*) Irregular distribution of junctional proteins in RPE. β-Catenin is located at the cell walls of RPE cells in a flat-mount preparation of a 12-month-old wild-type mouse. The cytoplasmic level of β-catenin increased (*), with reduced expression at the junctional sites (arrows). (*C*) A cross-section of the RPE of a 10-month-old wild-type mouse showing staining of the cell walls by β-catenin. An absence of β-catenin in the periphery and the increasing cytoplasmic level (*) are observed in a 10-month-old $Sod1^{-/-}$ mouse. (*D*) Distribution of N-cadherin in a 12-month-old $Sod1^{-/-}$ mouse is severely disrupted, which is in contrast to the hexagonal expressions of N-cadherin in an age-matched wild-type mouse. Incomplete expression at the junctional sites can be seen (arrows). (*E*) Quantification of cytoplasmic fluorescence intensity of β-catenin in RPE cells by using the digitalized images of the flat mounts of the wild-type and the $Sod1^{-/-}$ mice. Randomized selected cells ($n = 49$) of each group are compared. Results are shown as mean ± SEM. *, Statistical difference between the two groups ($P < 0.001$, Student's *t* test). (Scale bars: *A*, *B*, and *D*, 50 μm; *C*, 10 μm.)

been correlated with AMD (40), and no clear relationship has yet been demonstrated in the analysis of the RPE of patients with AMD (41, 42). These studies seem not to be conclusive because the number of subjects is limited. Studies of SOD1 activity in the RPE involving larger numbers of patients are needed to determine the causative role of SOD1 in the pathogenesis of human AMD. It is also possible that some human AMD patients carry underexpressing mutations of the SOD1 gene.

Genetic polymorphism of the SOD2 gene, on the other hand, has been associated with AMD (43). Although a retinal thinning has been observed in mice deficient in SOD2, they die soon after birth and therefore are not suited for use in studies of long-term age-related retinal changes (44, 45).

In conclusion, we have demonstrated that the lack of SOD1 leads to the development of an animal recapitulating drusen, CNV, and RPE dysfunction, which could be a platform to validate therapies for age-related retinal degenerative disorders including AMD. Because β-catenin is a key molecule in constituting the integrity of the RPE cell layer, further research will be necessary to elucidate the means by which SOD1 deficiency interferes with the dynamics of β-catenin in the RPE.

Methods

Mice. $Sod1^{-/-}$ mice on a C57BL/6 background were generated as described (46), and wild-type C57BL/6 mice were purchased from The Jackson Laboratory. Genotyping was performed by PCR as described (46). All animal experiments were performed in accordance with the Association for Research in Vision and Ophthalmology (ARVO) Statement for the Use of Animals in Ophthalmic and Visual Research.

Fundus Photography and Angiography. Fundus examinations were performed with an indirect ophthalmoscope (Heine Optotechnik, Herrsching, Germany) and a 28-diopter lens by two masked examiners independently. Pupils were fully dilated with 0.5% tropicamide and 0.5% phenylephrine-HCL (Santen, Osaka), the fundus was photographed with a charge-coupled device (CCD) camera (CS5130; Tokyo Electronic Industry, Tokyo), and these photographs were stored as digitalized images. Angiograms were taken with a small animal fundus camera (RC2; Kowa, Tokyo, Japan), and 60 μl of 5% sodium fluorescein (Alcon Laboratories, Fort Worth, TX) per animal was injected into the tail vein.

Immunohistochemistry. The enucleated mouse eyes were immersed immediately in optimal cutting temperature (OCT) compound (Lab-Tek) and frozen in dry ice–ethanol for immunohistochemical or hematoxylin and eosin staining. For fluorescent labeling, frozen sections (8 μm) were fixed in ice-cold acetone or 4% paraformaldehyde in PBS, blocked with rabbit or goat serum, and stained with rabbit Ab to human CD46 (Santa Cruz Biotechnology) (10), rabbit Ab to C5 (Abcam, Cambridge, MA), mouse Ab to mouse CML (TransGenic, Kumamoto, Japan), rabbit Ab to human TIMP3 (Lab Vision, Fremont, CA), goat Ab to human vitronectin (Santa Cruz Biotechnology) (47), rabbit Ab to 8-hydroxy-2′-deoxyguanosine (8-OHdG) (Nikken SEIL, Shizuoka, Japan), rabbit Ab to rat SOD1 (Stressgen Biotechnologies, Victoria, Canada), and rabbit Ab to human SOD2 (Stressgen Biotechnologies). The specificity of the selected Abs to mouse tissues was confirmed by Western blot analysis (C5, TIMP3, SOD1, and SOD2). The secondary Abs were anti-Ig Alexa Fluor 488 (Molecular Probes) to goat, mouse, or rabbit. For the immunostaining of 8-OHdG, images with positive reactions were merged with images from a light microscope.

Electron Microscopy. For transmission electron microscopy (TEM), tissues were fixed in 2.5% glutaraldehyde and then postfixed in 1% OsO_4. The fixed tissues were dehydrated and embedded in Quetol 812 and sectioned with a diamond knife. Quetol 812 sections (2 μm) were counterstained with toluidine blue and examined with a light microscope. Ultrathin sections (2 μm) were stained in 2% uranyl acetate and lead citrate and examined with an electron microscope (JEM-1200EX; JEOL).

Light Exposure. Five-month-old $Sod1^{-/-}$ and wild-type mice were exposed to constant white fluorescent light (Toshiba Lighting and Technology, Tokyo) in a light box surrounded by mirrors (Tinker-N, Kyoto, Japan) for 24 h per day for 8 weeks. Fundus examination was performed every 2 weeks. The light intensity was 10,000 lux. Digitalized fundus images were recorded from the eyes of $Sod1^{-/-}$ ($n = 25$) and wild-type ($n = 25$) mice, and the number of drusen was counted by two examiners masked to the type of animal.

Western Blot Analysis. Proteins extracted from the ocular tissues of 10- to 12-month-old $Sod1^{-/-}$ and wild-type mice were examined by Western blot using rabbit Abs to SOD1, SOD2, SOD3 (Stressgen Biotechnologies), and GAPDH (Biogenesis, Bournemouth, U.K.).

Flat-Mount Preparations and Digital Images. The enucleated eyes from 12-month-old $Sod1^{-/-}$ mice and age-matched wild-type mice ($n = 4$, each group) were sectioned at the equator, and the anterior half, including the lens and vitreous, was dis-

carded. The retinas were carefully peeled from the eyecup and optic nerve by using specialized scissors and forceps under a biomicroscope (SMZ-10; Nikon). The posterior eye segment containing the sclera and choroid was dissected into quarters by four radial cuts, mounted, and air-dried. Flat mounts were examined with a fluorescence microscope (BX51; Olympus, Melville, NY). The flat mounts were stained with mouse monoclonal Ab to β-catenin (Bioscience Laboratories, Bozeman, MT) or N-cadherin (Bioscience Laboratories), preconjugated with anti-mouse Ig Alexa Fluor 488 or 594 (Molecular Probes). Fluorescein images of β-catenin were analyzed after normalization to the background, and the degree of fluorescence of the cytoplasm of each cell was calculated from average pixel intensities by using commercial software (Adobe Photoshop CS; Adobe Systems, San Jose, CA).

Statistical Analyses. All data are presented as means ± SEM, and the differences were analyzed with Student's t test. P values <0.05 were considered statistically significant.

We thank Yuka Kondo, Manabu Hirasawa, Yutaka Ohta, Ei-ichiro Nagasaka, and Masao Yoshikawa for technical assistance; Yumi Takanashi, Naoko Takayasu, and Junko Moriya for assisting with histology; Minoru Seki for angiography; Murat Dogru, Yoji Takano, Catherine Oshima, and Duco Hamasaki for reviewing the manuscript; Yasushi Inaida for financial support; and Makoto Suematsu for critical comments in interpretation of data.

1. Sommer, A., Tielsch, J. M., Katz, J., Quigley, H. A., Gottsch, J. D., Javitt, J. C., Martone, J. F., Royall, R. M., Witt, K. A. & Ezrine, S. (1991) *N. Engl. J. Med.* **325,** 1412–1417.
2. Smith, W., Assink, J., Klein, R., Mitchell, P., Klaver, C. C., Klein, B. E., Hofman, A., Jensen, S., Wang, J. J. & de Jong, P. T. (2001) *Ophthalmology* **108,** 697–704.
3. Attbo, K., Mitchell, P. & Smith, W. (1996) *Ophthalmology* **103,** 357–364.
4. VanNewkirk, M. R., Weih, L., McCarty, C. A. & Taylor, H. R. (2001) *Ophthalmology* **108,** 960–967.
5. Oshima, Y., Ishibashi, T., Murata, T., Tahara, Y., Kiyohara, Y. & Kubota, T. (2001) *Br. J. Ophthalmol.* **39,** 367–372.
6. Bird, A. C., Bressler, N. M., Bressler, S. B., Chisholm, I. H., Coscas, G., Davis, M. D., de Jong, P. T., Klaver, C. C., Klein, B. E., Klein, R., *et al.* (1995) *Surv. Ophthalmol.* **39,** 367–374.
7. Smiddy, W. E. & Fine, S. L. (1984) *Ophthalmology* **91,** 271–277.
8. Wang, J. J., Foran, S., Smith, W. & Mitchell, P. (2003) *Arch. Ophthalmol.* **121,** 658–663.
9. Hahn, P., Qian, Y., Dentchev, T., Chen, L., Beard, J., Harris, Z. L. & Dunaief, J. L. (2004) *Proc. Natl. Acad. Sci. USA* **101,** 13850–13855.
10. Ambati, J., Anand, A., Fernandez, S., Sakurai, E., Lynn, B. C., Kuziel, W. A., Rollins, B. J. & Ambati, B. K. (2003) *Nat. Med.* **11,** 1390–1397.
11. Yoshida, T., Ohno-Matsui, K., Ichinose, S., Sato, T., Iwata, N., Saido, T. C., Hisatomi, T., Mochizuki, M. & Morita, I. (2005) *J. Clin. Invest.* **115,** 2793–2800.
12. Malek, G., Johnson, L. V., Mace, B. E., Saloupis, P., Schmechel, D. E., Rickman, D. W., Toth, C. A., Sullivan, P. M. & Bowes Rickman, C. (2005) *Proc. Natl. Acad. Sci. USA* **102,** 11900–11905.
13. Rackoczy, P. E., Zhang, D., Robertson, T., Barnett, N. L., Papadimitriou, J., Constable, I. J. & Lai, C.-M. (2002) *Am. J. Pathol.* **161,** 1515–1524.
14. Weng, J., Mata, N. L., Azarian, S. M., Tzekov, R. T., Birch, D. G. & Travis, G. H. (1999) *Cell* **98,** 13–23.
15. Rakoczy, P. E., Yu, M. J. T., Nusinowitz, S., Chang, B. & Heckenlively, J. R. (2006) *Exp. Eye Res.* **82,** 741–752.
16. Andersen, J. K. (2004) *Nat. Med.* **10,** S18–S25.
17. Harman, D. (1956) *J. Gerontol.* **11,** 298–300.
18. Beatty, S., Koh, H. H., Henson, D. & Boulton, M. (2000) *Surv. Ophthalmol.* **45,** 115–134.
19. Hahn, P., Milam, A. H. & Dunaief, J. L. (2003) *Arch. Ophthalmol.* **121,** 1099–1105.
20. Valentine, J. S., Doucette, P. A. & Potter, S. Z. (2005) *Annu. Rev. Biochem.* **74,** 563–593.
21. Behndig, A., Svensson, B., Marklund, S. L. & Karlsson, K. (1998) *Invest. Ophthalmol. Vis. Sci.* **39,** 471–475.
22. Hageman, G. S., Mullins, R. F., Russell, S. R., Johnson, L. V. & Anderson, D. H. (1999) *FASEB. J.* **13,** 477–484.
23. Johnson, L. V., Leitner, W. P., Staples, M. K. & Anderson, D. H. (2001) *Exp. Eye Res.* **73,** 887–896.
24. Kamei, M. & Hollyfield, J. G. (1999) *Invest. Ophthalmol. Vis. Sci.* **40,** 2367–2375.
25. Crabb, J. W., Miyagi, M., Gu, X., Shadrach, K., West, K. A., Sakaguchi, H., Kamei, M., Hasan, A., Yan, L., Rayborm, M. E., *et al.* (2002) *Proc. Natl. Acad. Sci. USA* **99,** 14682–14687.
26. Hageman, G. S., Luthert, P. J., Victor Chong, N. H., Johnson, L. V., Anderson, D. H. & Mullins, R. F. (2001) *Prog. Retin. Eye Res.* **20,** 705–732.
27. Haines, J. L., Hauser, M. A., Schmidt, S., Scott, W. K., Olson, L. M., Gallins, P., Spencer, K. L., Kwan, S. Y., Noureddine, M., Gilbert, L. R., *et al.* (2005) *Science* **308,** 419–421.
28. Edwards, A. O., Ritter, R., III, Abel, K. J., Manning, A., Panhuysen, C. & Farrer, L. A. (2005) *Science* **308,** 421–424.
29. Klein, R. J., Zeiss, C., Chew, E. Y., Tsai, J. Y., Sackler, R. S., Haynes, C., Henning, A. K., SanGiovanni, J. P., Mane, S. M., Mayne, S. T., *et al.* (2005) *Science* **308,** 385–389.
30. Cruickshanks, K. J., Klein, R., Klein, B. E. & Nondahl, D. M. (1993) *Arch. Ophthalmol.* **115,** 514–518.
31. Wenzel, A., Grimm, C., Samardzija, M. & Reme, C. E. (2005) *Prog. Retin. Eye Res.* **24,** 275–306.
32. Vingerling, J. R., Hoffman, A., Grobbee, D. E. & de Jong, P. T. (1996) *Arch. Ophthalmol.* **114,** 1193–1196.
33. Green, R. G. & Harlan, J. B. (1999) in *Age-Related Macular Degeneration*, eds. Berger, J. W., Fine, S. L. & Maguire, M. G (Mosby, St. Louis), pp. 81–154.
34. Kasai, H., Chung, M. H., Jones, D. S., Inoue, H., Ishikawa, H., Kamiya, H., Ohtsuka, E. & Nishimura, S. (1991) *J. Toxicol. Sci.* **16,** 95–105.
35. Ishibashi, T., Murata, T., Hangai, M., Nagai, R., Horiuchi, S., Lopez, P. F., Hinton, D. R. & Ryan, S. J. (1998) *Arch. Ophthalmol.* **116,** 1629–1632.
36. Bailey, T. A., Kanuga, N., Romero, I. A., Greenwood, J., Luthert, P. J. & Cheetham, M. E. (2004) *Invest. Ophthalmol. Vis. Sci.* **45,** 675–684.
37. Semkova, I., Peters, S., Welsandt, G., Janicki, H., Jordan, J. & Schraermeyer, U. (2003) *Invest. Ophthalmol. Vis. Sci.* **44,** 5349–5354.
38. Schwesinger, C., Tee, C., Rohan, R. M., Joussen, A. M., Fernandez, A., Meyer, T. N., Poulaki, V., Ma, J. J., Redmond, T. M., Liu, S., *et al.* (2001) *Am. J. Pathol.* **158,** 1161–1172.
39. Age-Related Eye Disease Study Research Group (2001) *Arch. Ophthalmol.* **119,** 1439–1452.
40. Delcourt, C., Cristol, J. P., Leger, C. L., Descomps, B. & Papoz, L. (1999) *Ophthalmology* **106,** 215–222.
41. Liles, M. R., Newsome, D. A. & Oliver, P. D. (1991) *Arch. Ophthalmol.* **109,** 1285–1288.
42. Frank, R. N., Amin, R. H. & Puklin, J. E. (1999) *Am. J. Ophthalmol.* **127,** 694–709.
43. Kimura, K., Isashiki, Y., Sonoda, S., Kakiuchi-Matsumoto, T. & Ohba, N. (2000) *Am. J. Ophthalmol.* **130,** 769–773.
44. Li, Y., Huang, T. T., Carlson, E. J., Melov, S., Ursell, P. C., Olson, J. L., Noble, L. J., Yoshimura, M. P., Berger, C., Chen, P. H., *et al.* (1995) *Nat. Genet.* **11,** 376–381.
45. Sandbach, J. M., Coscun, P. E., Grossniklaus, H. E., Kokoszka, J. E., Newman, N. J. & Wallace, D. C. (2001) *Invest. Ophthalmol. Vis. Sci.* **42,** 2173–2178.
46. Matzuk, M. M., Dionne, L., Guo, Q., Kumar, T. R., & Lebovitz, R. M. (1998) *Endocrinology* **139,** 4008–4011.
47. Teesalu, T. T., Hinkkanen, A. E. & Vaheri, A. (2001) *Am. J. Pathol.* **159,** 2227–2237.

Clinical and Experimental Ophthalmology 2006; 34: 491–499
doi:10.1111/j.1442-9071.2006.1253.x

Letters to the Editor

Clinical Case Notes

Microcirculation at optic disc rim is correlated with visual field defects in cases of anterior ischaemic optic neuropathy

ABSTRACT

We report two cases of anterior ischaemic optic neuropathy in whom tissue blood flow at the disc rim was correlated with the visual field defect. Tissue blood flow of each eye was evaluated with Heidelberg retina flowmeter. Both cases experienced acute visual loss and an altitudinal hemianopsia associated with optic disc oedema in the affected eye. In each case, the tissue blood flow at the affected (upper or lower half) disc rim corresponding to visual field deficit was reduced compared with that at the opposite-sided half disc rim in the affected eye and with the corresponding area in the fellow eye. The reduction of blood flow in the affected half disc rim associated with the visual field defect demonstrated that retina flowmetry can detect differences in tissue blood flow between superior and inferior sectional disc rim areas as well as between eyes non-invasively.

Key words: AION, microcirculation, visual field defect

INTRODUCTION

Anterior ischaemic optic neuropathy (AION) begins with acute visual disturbances and optic disc oedema. Fluorescein angiography shows some segmental delay or optic disc staining in the area corresponding with the visual field defect. Later, the affected segment of optic disc becomes atrophic and the visual field defect is irreversible. It has been hypothesized that AION results from a disturbance of the circulation on the optic nerve head (ONH) from an occlusion of a posterior ciliary artery.[1]

The Heidelberg retina flowmeter (HRF, Heidelberg Engineering Gmbh, Heidelberg, Germany) is designed for non-invasive measurements of retinal blood flow. Reproducible and quantitative measurements of capillary blood flow are possible in distinct areas of a capillary meshwork of the eye.[2]

We present two cases of AION in which HRF demonstrated a reduction of blood flow in the optic disc rim that corresponded with the visual field defect.

METHODS

The tissue blood flow was measured five times in a $10° \times 2.5°$ area in both eyes. The areas examined were the superior and inferior disc rim and the superior and inferior paramacular areas. Each area was made up of 256 points × 64 lines, and each line was scanned 128 times. The mean blood flow (MBF) was calculated as an indicator of tissue microcirculation by the automatic full-field perfusion image analyser (AFFPIA, version 3.3, Heidelberg Engineering GmbH).[3] The ratio of the MBF between the two eyes in normal subjects is approximately 1.0.[4] The MBF was obtained by averaging three values after omitting the highest and lowest ones. The ratio of the MBF of the affected eye to the fellow eye (A/F) was calculated for each area, and the ratio of the MBF in the superior disc rim to that in the inferior disc rim (S/I) was calculated.

CASE REPORT

Case 1: A 62-year-old man noticed a sudden loss of vision in his lower visual field of the right eye. He showed an altitudinal visual field defect in the right eye by Humphrey perimetry and was referred to our unit in September 2002. He had not had any visual problems or significant family history.

On examination, he did not have a relative afferent pupillary defect, and his eye movements were normal. His best-corrected visual acuity was 6/6 in both eyes, and the intraocular pressure was 14 mmHg in both eyes. The right optic disc was swollen (Fig. 1a), but the left fundus was completely normal. Both Humphrey and Goldmann perimetry showed an inferior altitudinal hemianopsia in the right eye (Fig. 1b). Fluorescein angiography revealed a marked delayed arm-to-retina circulation time (53.3 s) in the right eye, although delayed circulation time is not typical of non-arteritic AION. The right eye was diagnosed as having AION.

The A/F ratios in each area and the S/I ratios in each eye clearly demonstrate a reduction of blood flow in the superior disc rim in the right eye (Fig. 2) which corresponded with the visual field defect (Figs 1b,2a).

Case 2: A 47-year-old man noticed a superior visual field defect after vitrectomy for vitreous haemorrhage associated with proliferative diabetic retinopathy of the right eye in Keio University hospital. The surgery was performed under retrobulbar anaesthesia and no major complication was encountered. Intraoperative panretinal photocoagulation was performed, but neither gas nor air injection was done.

On examination, the light reflex and eye movements were normal. The best-corrected visual acuity was 6/9 in the right eye and 6/6 in the left eye. The intraocular pressure ranged 14–16 mmHg without any antiglaucomatous medication. Funduscopy revealed attenuated retinal arteries and oedematous change in the inferior portion of the optic disc in the right eye (Fig. 1c). Goldmann perimetry demonstrated a superior altitudinal hemianopsia in the right eye (Fig. 1d). Fluorescein angiography showed a mildly prolonged arm-to-retina time (21.0 s) and local hyperfluorescence in the right optic disc. Visual acuity improved to 6/6 but the optic disc became pale and a visual field defect remained 6 years after surgery.

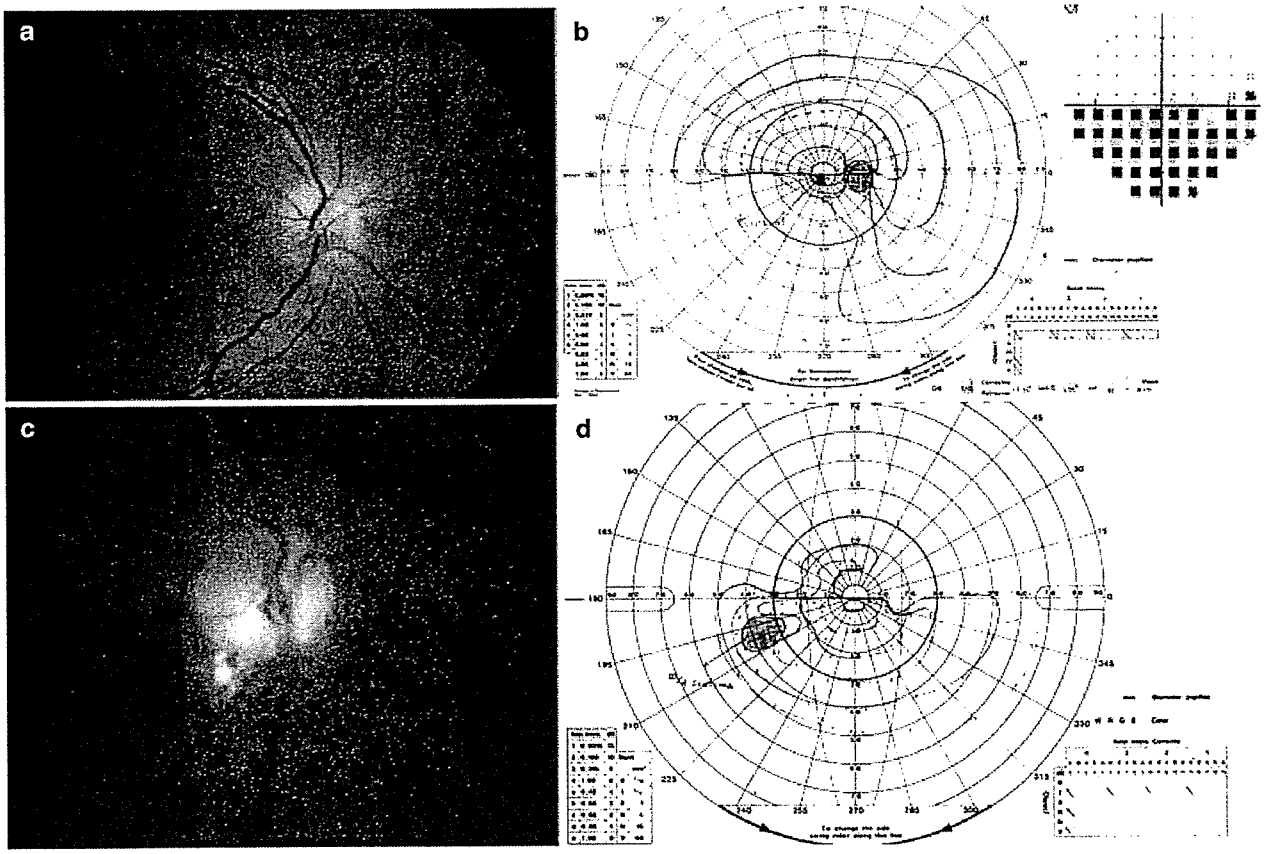

Figure 1. (a) Fundus photograph of the right eye in case 1 showing disc swelling. Sectional change is unclear. (b) Goldmann perimetry and Humphrey visual field of the right eye in case 1 showing inferior altitudinal hemianopsia. (c) Fundus photograph of the right eye in case 2 showing oedematous change in the inferior portion of the optic disc. (d) Goldmann perimetry of the right eye in case 2 showing superior altitudinal hemianopsia.

The A/F ratios in each area and the S/I ratios in each eye clearly demonstrate a reduction of blood flow in the inferior disc rim in the right eye (Fig. 2) which corresponded with the visual field defect (Figs 1d,2c).

Discussion

The main source of blood supply to the ONH is posterior ciliary artery circulation except for the surface nerve fibre layer which is supplied by the retinal circulation, and circulation pattern of the ONH has sectional distribution. It is generally believed that AION is due solely to non-perfusion or hypoperfusion of the ciliary circulation in the ONH, and not of the central retinal artery circulation in the ONH. Hayreh described that the primary objective of evaluating the ONH circulation in ischemia or vascular insufficiency of the ONH is to obtain information about the ciliary circulation in the prelaminar and deeper layers of the ONH and not the retinal circulation in the surface nerve fibre layer.[1] Flow values of disc rim obtained by HRF is considered to be a mixture of retinal and choroidal blood flow contribution because the depth of laser penetration is about 400 μm, thereby the scanning depth contains nerve fibre layer and prelaminar region. HRF measurements can be considered to be a suitable indicator closely related to the physiological status of retinal nerve fibre layer and neighbouring retinal ganglion cells. The juxtapapillary retinal blood flow was reported to be reduced in association with the structural damage of ONH in glaucoma patients by utilizing HRF.[5] The MBF measurements in our case clearly illustrated the specific circulation disturbance at the superior or inferior disc rim in the diseased eye, which corresponded with the ophthalmoscopic changes and the visual field deficit. Leiba *et al.* reported reduced microcirculation at ONH in association with altitudinal visual field defects in cases of AION by using HRF in the first place.[6] Our results reinforced their report and showed the convenience of analysis of microcirculation by using AFFPIA software.

In conclusion, our findings demonstrated that the AFFPIA for HRF instrument is a useful software for evaluating sectional ONH tissue blood flow, and can detect changes even not visible ophthalmoscopically.

Shinsuke Yokoyama MD,[1] Itaru Kimura MD,[1] Hisao Ohde MD,[1] Kei Shinoda MD[1,2] and Yukihiko Mashima MD[1]

[1]Department of Ophthalmology, Keio University School of Medicine, and [2]Laboratory of Visual Physiology, National Institute of Sensory Organs, Tokyo, Japan

Received 11 May 2005; accepted 5 December 2005.

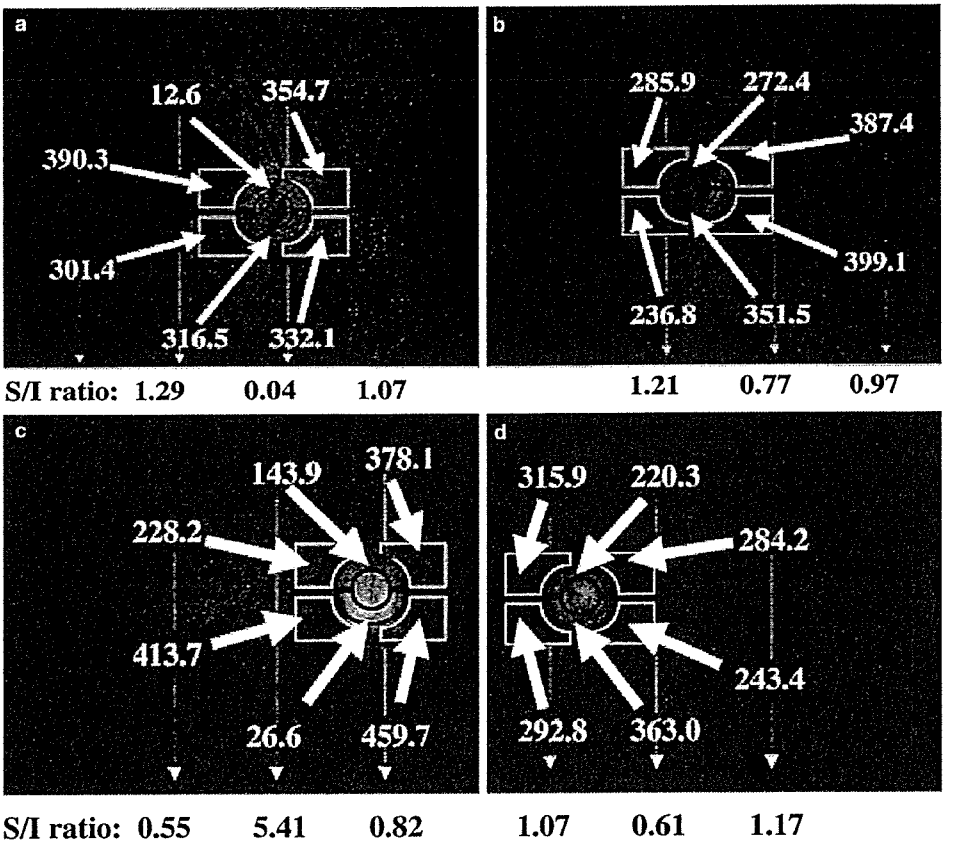

Figure 2. Mean blood flow (MBF) measurements of the disc rim and peripapillary retinal area. The area is divided into superior and inferior regions. The sectional tissue blood circulation disturbance in the superior disc rim area in the right eye was observed. MBF is indicated in arbitrary units. (a) and (b) show right and left eyes in case 1, and (c) and (d) show right and left eyes in case 2, respectively.

References

1. Hayreh SS. The blood supply of the optic nerve head and the evaluation of it – myth and reality. *Prog Retin Eye Res* 2001; 20: 563–93.
2. Michelson G, Schmauss B. Two dimensional mapping of the perfusion of the retina and optic nerve head. *Br J Ophthalmol* 1995; 79: 1126–32.
3. Michelson G, Welzenbach J, Pal I, Harazny J. Automatic full field analysis of perfusion images gained by scanning laser Doppler flowmetry. *Br J Ophthalmol* 1998; 82: 1294–300.
4. Kimura I, Shinoda K, Tanino T, Ohtake Y, Mashima Y, Oguchi Y. Scanning laser Doppler flowmeter study of retinal blood flow in macular area of healthy volunteers. *Br J Ophthalmol* 2003; 87: 1469–73.
5. Logan JF, Rankin SJ, Jackson AJ. Retinal blood flow measurements and neuroretinal rim damage in glaucoma. *Br J Ophthalmol* 2004; 88: 1049–54.
6. Leiba H, Rachmiel R, Harris A, Kagemann L, Pollack A, Zalish M. Optic nerve head blood flow measurements in non-arteritic anterior ischaemic optic neuropathy. *Eye* 2000; 14: 828–33.

Chemo-paralysis for the removal of a live intraocular worm in ocular angiostrongyliasis

Abstract

Angiostrongylus cantonensis is also called the rodent lung worm. It was first discovered in 1935 by Chen in Rattus *rattus*, in Canton, China. The rodent is the definitive host while infected mollusks, snails and crabs act as the intermediate hosts. Humans are infected by the 3rd stage larvae, either by eating undercooked intermediate hosts or by consuming vegetables.[1] It is a delicate nematode reported in Asia Pacific region most commonly in South-east Asia and has been reported from Taiwan, Thailand, Indonesia, Vietnam and Sri Lanka.[2] Anterior chamber angiostrogyliasis is extremely rare, and no previous case of ocular angiostrogyliasis from India could be found on Medline search. We report a new technique in the removal of the actively motile thread-like worm by paralysing it with intracameral preservative free lidocaine, which aids in the easy removal of the intact worm.

Key words: chemo-paralysis, ocular, angiostrongylus cantonensis

Case report

A 12-year-old boy presented with a 2-week history of diffuse pain, redness and gradual loss of vision in his left eye. He was in good health and denied any systemic complaints.

Available online at www.sciencedirect.com
SCIENCE DIRECT
Vision Research 46 (2006) 2675–2690
Vision Research
www.elsevier.com/locate/visres

Visual resolution with retinal implants estimated from recordings in cat visual cortex

Reinhard Eckhorn [a,*], Marcus Wilms [a], Thomas Schanze [a], Marcus Eger [a], Lutz Hesse [a,b], Ulf T. Eysel [c], Zoltán F. Kisvárday [c,1], Eberhart Zrenner [d], Florian Gekeler [d], Helmut Schwahn [d], Keisuke Shinoda [d], Helmut Sachs [e], Peter Walter [f]

[a] *Department of Physics, Neurophysics Group, Philipps-University Marburg, Germany*
[b] *Eye Clinic, Philipps-University Marburg, Germany*
[c] *Department of Neurophysiology, Medical Faculty, Ruhr-University Bochum, Germany*
[d] *University Eye Hospital, Medical Faculty, University of Tübingen, Germany*
[e] *University Eye Hospital, Medical Faculty, University of Regensburg, Germany*
[f] *University Eye Hospital, Medical Faculty, University of Aachen, Germany*

Received 14 May 2005; received in revised form 7 January 2006

Abstract

We investigated cortical responses to electrical stimulation of the retina using epi- and sub-retinal electrodes of 20–100 μm diameter. Temporal and spatial resolutions were assessed by recordings from the visual cortex with arrays of microelectrodes and optical imaging. The estimated resolutions were ~40 ms and ~1° of visual angle. This temporal resolution of 25 frames per second and spatial resolution of about 0.8 cm at about 1 m and correspondingly 8 cm at 10 m distance seems sufficient for useful object recognition and visuo-motor behavior in many in- and out-door situations of daily life.

Keywords: Retina prosthesis; Visual cortex; Spatial and temporal resolution; Electrical stimulation

1. Introduction

Retinal photoreceptors transform visual stimuli into electrical signals in normal vision. These signals are processed by intraretinal neural networks and the resulting visual information is submitted by retinal ganglion cells to subsequent visual centers. This is not so in the case of diseases of the outer retina, including macula degeneration and retinitis pigmentosa. They lead to a progressive and finally total loss of the photoreceptors. However, a large percentage of inner retinal neurons remain histologically intact (Santos et al., 1997). In particular, a large number of the retinal ganglion cells stay functionally alive and can transmit action potentials via the optic tract. Apart from the substitution of retinal function by replacing deteriorated outer retinal cells with intact sub-retinal transplants (Seiler, Aramant, & Ball, 1999), most current concepts for restituting retinal functions are based on the electrical stimulation of the remaining intact visual neurons. Electrical stimuli are meant to coarsely mimic visual inputs to subsequent visual processing.

1.1. Previous work

In recent years, two main types of retinal implants have been developed using either sub-retinal or epi-retinal

* Corresponding author. Fax: +49 6421 282 70 34.
E-mail addresses: eckhorn@staff.uni-marburg.de, reinhard.eckhorn@physik.uni-marb (R. Eckhorn).
[1] Present address: University of Debrecen, Department of Anatomy, Histology and Embryology, Hungary.

0042-6989/$ - see front matter © 2006 Elsevier Ltd. All rights reserved.
doi:10.1016/j.visres.2006.01.034